Longitudinal progression of grey matter atrophy in non-amnestic Alzheimer's disease

*Jeffrey S. Phillips, PhD[1,2], *Fulvio Da Re, MD[1,3,4], David J. Irwin, MD[1,2], Corey T. McMillan, PhD[1,2], Sanjeev N. Vaishnavi, MD, PhD[2,5], Sharon X. Xie, PhD[6], Edward B. Lee, MD, PhD[7], Philip A. Cook, PhD[8], James C. Gee, PhD[8], Leslie M. Shaw, PhD[7], John Q. Trojanowski, MD, PhD[7], David A. Wolk, MD[2,5] and Murray Grossman, MD, EdD[1,2]

February 13, 2019

* These authors contributed equally to this work.

Short title: Longitudinal Atrophy in Non-Amnestic AD

Affiliations:

[1]Penn Frontotemporal Degeneration Center, University of Pennsylvania, Philadelphia, PA, USA, [2]Department of Neurology, Perelman School of Medicine, University of Pennsylvania, Philadelphia, PA, USA, [3]PhD Program in Neuroscience, University of Milano-Bicocca, Milan, Italy, [4]School of Medicine and Surgery, Milan Center for Neuroscience (NeuroMI), University of Milano-Bicocca, Milan, Italy, [5]Penn Memory Center, University of Pennsylvania, Philadelphia, PA, USA, [6]Department of Biostatistics, Epidemiology, and Informatics, Perelman School of Medicine, University of Pennsylvania, Philadelphia, PA, USA, [7]Center for Neurodegenerative Disease Research, University of Pennsylvania, Philadelphia, PA, USA, [8]Penn Image Computing and Science Laboratory, Department of Radiology, University of Pennsylvania, Philadelphia, PA, USA

Corresponding author:

Jeffrey S. Phillips, PhD
jefphi@pennmedicine.upenn.edu
Penn Frontotemporal Degeneration Center
Department of Neurology
University of Pennsylvania
3400 Spruce St., 3 Gibson
Philadelphia, PA 19104

Abstract

Recent models of Alzheimer's disease progression propose that disease may be transmitted between brain areas either via local diffusion or long-distance transport via white-matter fiber pathways. However, it is unclear whether such models are applicable in non-amnestic Alzheimer's disease, which is associated with domain-specific cognitive deficits and relatively spared episodic memory. To date, the anatomical progression of disease in non-amnestic patients remains understudied. We used longitudinal imaging to differentiate earlier atrophy and later disease spread in three non-amnestic variants, including logopenic-variant primary progressive aphasia (n=25), posterior cortical atrophy (n=20), and frontal-variant Alzheimer's disease (n=12), as well as 17 amnestic Alzheimer's disease patients. Patients were compared to 37 matched controls. All patients had autopsy (n=7) or cerebrospinal fluid (n=67) evidence of Alzheimer's disease pathology. We first assessed atrophy in suspected sites of disease origin, adjusting for age, sex, and severity of cognitive impairment; we then performed exploratory whole-brain analysis to investigate longitudinal disease spread both within and outside these regions. Additionally, we asked whether each phenotype exhibited more rapid change in its associated disease foci than other phenotypes. Finally, we investigated whether atrophy was related to structural brain connectivity. Each non-amnestic phenotype displayed unique patterns of initial atrophy and subsequent neocortical change that correlated with cognitive decline. Longitudinal atrophy included areas both proximal to and distant from sites of initial atrophy, suggesting heterogeneous mechanisms of disease spread. Moreover, regional rates of neocortical change differed by phenotype. Logopenic-variant patients exhibited greater initial atrophy and more rapid longitudinal change in left lateral temporal areas than other groups. Frontal-variant patients had pronounced atrophy in left insula and middle frontal gyrus, combined with more rapid atrophy of left insula than other non-amnestic patients. In the medial temporal lobes, non-amnestic patients had less atrophy at their initial scan than amnestic patients, but longitudinal rate of change did not differ between patient groups. Medial temporal sparing in non-amnestic Alzheimer's disease may thus be due in part to later onset of medial temporal degeneration than in amnestic patients rather than different rates of atrophy over time. Finally, the magnitude of longitudinal atrophy was predicted by structural connectivity, measured in terms of node degree; this result provides indirect support for the role of long-distance fiber pathways in the spread of neurodegenerative disease.

Keywords

Abbreviations

Aβ = β-amyloid; aAD= amnestic Alzheimer's disease; naAD = non-amnestic Alzheimer's disease; CBS = corticobasal syndrome; fvAD = frontal-variant Alzheimer's disease; lvPPA = logopenic-variant primary progressive aphasia; PCA = posterior cortical atrophy; GM = grey matter; MTL = medial temporal lobes; ROI = region of interest; MMSE = Mini Mental Status Exam; CSF = cerebrospinal fluid; LME = linear mixed effects; PVLT = Philadelphia Verbal Learning Test; PBAC = Philadelphia Brief Assessment of Cognition

Introduction

Recent theories of neurodegenerative disease progression have raised the possibility that pathogenic protein aggregates do not arise spontaneously throughout the brain; rather, they may be transmitted from areas of existing pathology through one or more mechanisms, including local diffusion of pathogenic proteins through the extracellular medium as well as long-distance transmission along white-matter pathways between brain areas (Guo and Lee, 2014). This transmission model of neurodegenerative disease is supported by a diverse body of research ranging from rodent models (Liu *et al.*, 2012; Iba *et al.*, 2013; Ahmed *et al.*, 2014; Mezias *et al.*, 2017) to computational modeling of human neuroimaging data (Raj *et al.*, 2012, 2015; Iturria-Medina *et al.*, 2014; Hu *et al.*, 2016). This research particularly supports the relevance of the transmission model in typical, amnestic Alzheimer's disease (AD), which spreads from the transentorhinal cortex and hippocampus to the rest of the medial temporal lobes and ultimately to the neocortex (Braak and Braak, 1991). This stereotyped progression provides detailed expectations against which to test models of interregional transmission.

However, it is unclear whether the transmission hypothesis has equal relevance in atypical presentations of AD, which demonstrate a number of pathological and clinical differences from amnestic AD (aAD), including relatively prominent neocortical disease and relative hippocampal sparing (Galton *et al.*, 2000; Murray *et al.*, 2011; Whitwell *et al.*, 2012; Mesulam *et al.*, 2014a). Clinically, atypical AD includes at least four non-amnestic phenotypes: logopenic-variant primary progressive aphasia (lvPPA), characterized by primary language deficits (Gorno-Tempini *et al.*, 2011); posterior cortical atrophy (PCA), characterized by visuospatial deficits (Crutch *et al.*, 2017); a variant defined by deficits in executive function and/or social behavior (Dubois *et al.*, 2014), frequently referred to as frontal-variant Alzheimer's disease (fvAD); and corticobasal syndrome (CBS), which can present with a constellation of lateralized motor and cognitive deficits (Medaglia *et al.*, 2017). These syndromes are marked by different rates of clinical progression than in aAD (Duara *et al.*, 2013; Byun *et al.*, 2015; Poulakis *et al.*, 2018). Moreover, each phenotype is associated with distinct anatomical distributions of disease, particularly in early stages. LvPPA patients have strongly left-lateralized disease with pathological accumulations in left superior temporal and inferior parietal cortex (Mesulam *et al.*, 2014b; Giannini *et al.*, 2017); additional disease is commonly observed in left dorsolateral prefrontal cortex (Rogalski *et al.*, 2016; Giannini *et al.*, 2017). PCA is marked by involvement of the parietal and/or occipital lobes (Tang-Wai *et al.*, 2004; Crutch *et al.*, 2017); depending on the patient, disease in PCA may or may not have a right-hemisphere bias (Crutch *et al.*, 2012; Ossenkoppele *et al.*, 2015a). In fvAD, elevated pathology has been most commonly reported in the frontal lobes (Johnson *et al.*, 1999; Blennerhassett *et al.*, 2014), although a recent report based on a larger sample of these patients also highlights disease in posterior cortical areas (Ossenkoppele *et al.*, 2015b). In CBS due to AD, disease is distributed widely and often asymmetrically throughout the temporal and parietal lobes, sometimes extending into the posterior portion of the frontal lobes (Lee *et al.*, 2011; McMillan *et al.*, 2016). Each of these naAD phenotypes shares clinical similarities to presentations of frontotemporal lobar degeneration (FTLD) spectrum pathology, making it imperative to corroborate clinical diagnosis through AD biomarkers.

Non-amnestic syndromes with underlying Alzheimer's disease pathology may be more prevalent than previously thought (Peter *et al.*, 2014; Dickerson *et al.*, 2017). However, relatively little research has examined the anatomical spread of non-amnestic Alzheimer's disease (naAD). In a previous MRI analysis (Phillips *et al.*, 2018), we inferred patterns of atrophy spread in naAD phenotypes from cross-sectional MRI data: following the logic of postmortem pathology studies, we explicitly assumed that the relative frequency of atrophy in different brain areas could be used to infer the anatomical progression of disease over time. These results corroborated the hypothesis that each naAD phenotype has a distinct neocortical origin with relative sparing of the medial temporal lobes (MTL). Moreover, this study suggested that each naAD phenotype has a distinct pattern of disease spread that differs from aAD.

In the present study, we sought to validate and extend this previous work, using longitudinal MRI to differentiate patterns of earlier atrophy from subsequent disease spread in each phenotype. Additionally, we investigated whether aAD and naAD differ in the anatomic distribution and longitudinal rate of grey matter (GM) atrophy over time. We reasoned that such differences could explain phenotype-specific patterns of clinical progression across amnestic and non-amnestic Alzheimer's disease variants. In a hypothesis-driven analysis based on our previous cross-sectional study (Phillips *et al.*, 2018), we investigated differences in GM

volume at the time of initial MRI as well as volume change over time in regions-of-interest (ROIs) associated with lvPPA, PCA, fvAD, and aAD. Exploratory, whole-brain, voxelwise analysis of cortical thickness was performed to map patterns of disease spread beyond these initial ROIs. We sought to identify group differences in atrophy distribution and progression independent of age, which has been previously reported to differ between typical and atypical forms of Alzheimer's disease (Murray *et al.*, 2011). Based on the high neocortical disease burden and domain-specific cognitive deficits that we previously observed in naAD, we predicted that naAD patients would exhibit faster rates of atrophy in phenotype-specific neocortical ROIs relative to aAD. Additionally, we tested the hypothesis that naAD patients would exhibit slower atrophy than aAD patients in the hippocampus and surrounding MTL areas, as a possible explanation for the relative memory sparing associated with these structures in naAD. Finally, we compared longitudinal atrophy patterns to measures of inter-regional structural connectivity estimated from a large population of healthy controls; we predicted that connectivity would predict longitudinal atrophy, consistent with the transmission hypothesis.

Materials and methods

Patients

Table 1: Participant characteristics at time of first scan. Median values and interquartile ranges (square brackets) are given for all continuous variables. Education, age at MRI, inter-scan interval, and disease duration are expressed in years. For each cognitive score, numbers in parentheses indicate the number of observations per group. P-values reflect the results of a chi-squared test for sex and Kruskal-Wallis tests for all other variables.

	Control	aAD	lvPPA	PCA	fvAD	P
N	37	17	25	20	12	
Male	16 (43.2%)	6 (35.3%)	9 (36.0%)	7 (35.0%)	7 (58.3%)	0.672
Education	16.0 [16.0, 18.0]	16.0 [14.0, 18.0]	16.0 [14.0, 19.0]	16.0 [12.0, 16.0]	16.0 [13.5, 18.0]	0.421
Age at MRI (years)	61.9 [57.9, 65.6]	59.4 [53.5, 70.3]	58.5 [56.9, 64.5]	58.0 [55.1, 61.4]	63.9 [59.7, 69.5]	0.137
Inter-scan interval (years)	1.2 [0.9, 1.7]	1.2 [0.9, 1.5]	1.1 [0.9, 1.3]	1.0 [0.9, 1.2]	1.0 [0.7, 1.1]	0.162
Disease duration (years)	—	3.0 [1.9, 4.0]	2.7 [1.7, 3.9]	2.2 [1.3, 4.0]	2.2 [1.8, 5.2]	0.747
MMSE (0–30)	29.0 [28.0, 30.0] (20)	23.0 [20.0, 25.0] (17)	25.0 [23.0, 28.0] (25)	24.5 [18.8, 25.2] (20)	23.0 [17.0, 26.0] (12)	<0.001
Recognition memory (discrimination, 0–1)	1.0 [0.9, 1.0] (7)	0.6 [0.5, 0.7] (10)	0.8 [0.8, 1.0] (25)	0.7 [0.6, 0.9] (19)	0.6 [0.6, 0.8] (12)	<0.001
Speech (0–4)	4.0 [4.0, 4.0] (3)	2.5 [2.5, 3.0] (9)	2.5 [2.0, 3.0] (19)	3.0 [3.0, 4.0] (15)	3.5 [2.2, 4.0] (11)	0.004
Letter fluency (# words/60 s)	19.0 [17.5, 20.5] (7)	9.0 [5.0, 13.0] (13)	8.5 [5.2, 10.8] (22)	10.0 [6.5, 15.5] (19)	6.5 [3.0, 11.0] (12)	0.001
Forward digit span (length correct)	7.0 [7.0, 8.0] (11)	5.0 [3.0, 6.0] (9)	5.0 [4.0, 5.0] (25)	6.0 [5.0, 7.0] (20)	5.0 [4.0, 6.0] (12)	0.005
Rey figure copy (0–12)	12.0 [12.0, 12.0] (3)	11.0 [4.0, 12.0] (9)	12.0 [11.0, 12.0] (19)	2.5 [0.0, 8.8] (12)	9.5 [4.5, 11.0] (10)	0.001
Judgment of line orientation (0–6)	6.0 [6.0, 6.0] (3)	3.0 [0.8, 5.0] (8)	5.0 [4.0, 6.0] (19)	2.0 [0.0, 4.0] (13)	4.0 [3.0, 5.0] (9)	0.004
Social behavior (0–18)	17.0 [17.0, 17.0] (3)	17.5 [16.8, 18.0] (8)	18.0 [17.0, 18.0] (19)	17.0 [16.0, 18.0] (15)	13.0 [11.1, 16.5] (11)	0.004
Oral trail-making test (0–6)	6.0 [5.5, 6.0] (3)	0.0 [0.0, 3.0] (5)	2.0 [0.2, 3.0] (10)	0.5 [0.0, 2.8] (10)	2.0 [0.2, 3.8] (6)	0.051
Reverse digit span (length correct)	6.0 [4.5, 6.0] (11)	3.0 [3.0, 3.0] (9)	3.0 [3.0, 4.0] (25)	3.0 [2.0, 3.0] (19)	3.0 [2.0, 3.2] (12)	<0.001

The current study used a longitudinal case-control design based on data retrospectively selected from the Integrated Neurodegenerative Disease Database at the University of Pennsylvania. Participants were recruited through the Penn Frontotemporal Degeneration Center (FTDC) and the Penn Memory Center (PMC). All procedures were approved by the University of Pennsylvania's Institutional Review Board, and all patients and/or their caregivers gave written informed consent according to the principles established by the Declaration of Helsinki. An initial database query yielded 1897 patients scanned on the same 3-Tesla Siemens MRI scanner at the Hospital of the University of Pennsylvania. Of these, 360 patients had either autopsy or cerebrospinal fluid biomarker evidence of underlying Alzheimer's disease pathology. An additional 58 patients were excluded due to major cerebrovascular disease, stroke, head trauma, or comorbid psychiatric, neurodegenerative, medical, or developmental disorders apart from their primary diagnoses. Of the remainder, a total of 90 patients had longitudinal data available and exhibited clinical phenotypes of interest, as described below. At time of recruitment, MRI scans for all patients were screened for signs of cerebrovascular disease, hydrocephalus, or white matter lesions; those with a Fazekas scale score>1 were excluded. Additionally, MRI scans were visually inspected by two raters (JSP and FDR), and 16 patients were excluded for poor quality data. The final sample included 181 T1-weighted MRI scans from 74 patients (25 with lvPPA, 20 PCA, 12 with fvAD, and 17 with aAD) and 85 scans from 37 demographically-matched controls. A majority of participants (48/74 patients and 29/37 controls) had only 2 available scans; the remaining participants

contributed 3–4 scans each. We included scans acquired with a minimum inter-scan interval of 6 months up to 3.5 years from the initial MRI; beyond this window, there were insufficient observations for a valid analysis. Seven patients had primary neuropathologic diagnoses and 67 had CSF biomarkers (total tau/beta-amyloid ratio greater than 0.34) indicative of Alzheimer's disease pathology according to methods previously described (Shaw *et al.*, 2009; Irwin *et al.*, 2012; Toledo *et al.*, 2012). APOE genotyping was performed on 66 of 74 patients. One patient (white male, aAD, age 51 at onset) with an APOE $\epsilon 3/\epsilon 4$ genotype was found to have a mutation in the PSEN1 gene; supplementary analyses indicated that excluding this patient did not have substantive effects on the outcome of key analyses. All patients were clinically diagnosed by experienced neurologists (MG, DJI, DW, and SV), and diagnoses were confirmed by consensus after patients' initial visit by clinicians with expertise in dementia. Clinical criteria for each patient phenotype were as follows: for lvPPA, primary language impairment including deficits in repetition and/or naming (Gorno-Tempini *et al.*, 2011; Giannini *et al.*, 2017); for PCA, visuospatial deficits (e.g., in object/spatial perception, neglect, or oculomotor apraxia) (Crutch *et al.*, 2017); for fvAD, clinical evidence of a behavioral/dysexecutive syndrome per Rascovsky et al.'s (2011) criteria for behavioral-variant frontotemporal dementia; and for aAD, primary memory impairment plus deficits in one or more additional cognitive domains (McKhann *et al.*, 2011). NaAD patients had relatively preserved episodic memory, as assessed through clinical interviews and detailed mental status examinations; however, we note that the label "non-amnestic" is used throughout this manuscript to denote patients' initial presentation and does not preclude the development of memory deficits in more advanced disease. NaAD patients also had relatively spared abilities in other cognitive domains except their domain of primary impairment at initial presentation. Due to the challenges of clinically differentiating behavioral/dysexecutive syndromes due to AD vs. FTLD, we performed additional screening on the fvAD group, as detailed in the Supplementary Material ("Patient selection details"). The current study included 54 patients from our previous, cross-sectional study (Phillips *et al.*, 2018) (aAD, n=8; lvPPA, n=24; PCA, n=16; and fvAD, n=6).

Shapiro-Wilks tests indicated non-normal distributions for education and disease duration, age, and MMSE score at initial MRI (all p<0.001). Kruskal-Wallis tests of group differences were non-significant, with the exception of MMSE [$\chi^2(4)=38.5$, p<0.001], reflecting patients' cognitive deficits relative to controls. Mann-Whitney tests confirmed that all patient groups exhibited significantly lower MMSE scores than controls (all U>=428, p<0.001); all other pairwise comparisons were non-significant. To corroborate naAD patients' domain-specific cognitive impairment, we analyzed neuropsychological performance on assessments independent of those used in clinical diagnosis, including performance on specific items of the Philadelphia Brief Assessment of Cognition (PBAC) (Libon *et al.*, 2011b). Only neuropsychological observations acquired within 1 year of an MRI scan were included. Language was assessed in terms of speech features (with lower scores indicating speech and language impairment), forward digit span as a measure of repetition (Giannini *et al.*, 2017), and letter fluency, which is sensitive to deficits in executive-mediated lexical retrieval (Rascovsky *et al.*, 2007; Ramanan *et al.*, 2017). Visuospatial function was assessed by patients' ability to copy a modified version of the Rey complex figure as well as the judgment of line orientation. Social behavior was assessed on an 18-point scale evaluating social comportment, apathy, disinhibition, agitation, empathy, and ritualistic behaviors. Executive function was evaluated through an oral version of the trail-making test as well as backward digit span. Finally, episodic memory was assessed by recognition on the Philadelphia Verbal Learning Test (PVLT) (Libon *et al.*, 2011a) or the PBAC verbal memory test, as available. All neuropsychological assessments were acquired within 1 year of the initial MRI scan (PVLT: mean=0.19 years, SD=0.25; letter fluency: mean=0.14 years, SD=0.25; PBAC: mean=0.21 years, SD=0.27; digit span: mean=0.11 years, SD=0.21). Results were consistent with each phenotype's primary impairment in all domains except for executive function (Table 1). Post-hoc comparisons between patient groups for neuropsychological performance at initial MRI are reported in Supplementary Table 11. The median and maximum follow-up intervals for the MMSE were 1.4 and 3.8 years, respectively; for verbal recognition memory, 1.7 and 4.2 years; for letter fluency, 1.6 and 4.6 years; for forward and reverse digit span, 1.5 and 4.0 years; and for additional measures, which were derived from the PBAC, 1.6 and 4.6 years.

4

Neuroimaging methods

T1-weighted MR images were acquired axially with 0.98 mm x 0.98 mm x 1 mm voxels, a 256 x 192 matrix, a repetition time of 1620 ms, an inversion time of 950 ms, and a flip angle of 15°. Scans were visually inspected for quality by two authors (JP and FDR). Advanced Normalization Tools (ANTs) (Avants *et al.*, 2014; Tustison *et al.*, 2014) was used to process each image using a prior-based approach. Images underwent intensity normalization (Tustison *et al.*, 2010) and were spatially normalized to a template based on healthy controls from the Open Access Series of Imaging Studies (OASIS) dataset (Marcus *et al.*, 2007) using a symmetric diffeomorphic algorithm (Klein *et al.*, 2009; Avants *et al.*, 2011). Images were segmented into 6 tissue classes (cortical grey matter, subcortical grey matter, deep white matter, CSF, brainstem, and cerebellum) using template-based priors; this tissue segmentation was then used to estimate cortical thickness; ANTs cortical thickness measurements have been extensively validated relative to surface-based methods such as FreeSurfer (Tustison *et al.*, 2014; Klein *et al.*, 2017). We used a joint label fusion approach (Wang *et al.*, 2013) to align the Mindboggle-101 labels (based on the Desikan-Killainy-Tourville label scheme) (Klein and Tourville, 2012) with each image using pseudo-geodesic registration (Tustison and Avants, 2013) and calculated the volume of GM voxels within each label, normalized by intracranial volume and converted to a z-score relative to controls' initial scans. To perform voxelwise group analyses, we warped cortical thickness images to the template using the previously-computed spatial transforms; these images were then spatially smoothed with a 2-sigma Gaussian kernel and downsampled to 2 mm isotropic voxels.

Statistical analysis

In a hypothesis-driven analysis, we analyzed GM volumes in phenotype-specific ROIs motivated by our previous study of disease progression in naAD (Phillips *et al.*, 2018). This study identified the regions most commonly atrophied in each naAD phenotype, reflecting the likely anatomical origin of disease. These ROIs included left middle and superior temporal gyri in lvPPA; right precuneus, superior parietal lobule, and angular, supramarginal, and middle temporal gyri in PCA; and left anterior insula and middle frontal gyrus as well as right middle temporal gyrus in fvAD (Table 2). Each ROI was expected to exhibit lower volume at the time of participants' initial MRI scan as well as more rapid volume loss over time in its associated patient group(s) relative to other groups. We additionally hypothesized that the aAD group would demonstrate selective atrophy in the MTL, including bilateral hippocampi, parahippocampal gyri, and entorhinal cortex. Atrophy at the time of initial MRI was analyzed using multiple linear regression models with a factor of group and covariates for age, sex, and MMSE score at the time of initial MRI; controls formed the reference group in these models. Longitudinal atrophy was assessed using linear mixed effects (LME) models with fixed factors of group, time since first scan, and the interaction of group x time. As in the baseline model, covariates included age, sex, and MMSE score at initial MRI. A subject-specific random intercept was included to account for intra-individual correlations in imaging measures. Post-hoc comparisons were performed for the effect of group at initial MRI as well as the group x time interaction in longitudinal models; values of p<0.05, corrected using the false discovery rate method, were considered significant.

We used LME models to relate GM volume change to neuropsychological performance within 1 year of each imaging session. Due to the limited number of observations, only linear associations between atrophy and time were assessed. The mean interval between test and MRI was 0.30 years (SD=0.30) for recognition memory; 0.22 years (SD=0.29) for letter fluency; 0.18 years (SD=0.29) for digit span; and 0.25 years (SD=0.33) for all other longitudinal neuropsychological measures. Separate LME models were computed for each measure and change in associated ROIs. Thus, recognition performance was related to GM volume in each of the 6 MTL ROIs; language measures were compared to volume change in left middle and superior temporal gyrus; visuospatial measures were related to change in the right superior parietal lobule, precuneus, and angular, supramarginal, and middle temporal gyri; and behavioral and executive measures were related to left anterior insula and middle frontal gyrus as well as right middle temporal gyrus. Neuropsychological performance formed the outcome in each model; predictors treated as fixed effects included regional GM volume at initial MRI and subsequent volume change, as well as covariates of sex and education. Additionally, a subject-specific random intercept was included in the LME model. Due to limited neuropsychological data,

controls were omitted from these models. The association with regional volume change in each model was assessed at a significance level of p<0.05, corrected for false discovery rate.

Additionally, we performed exploratory, whole-brain, voxelwise analysis to investigate differences in cortical thickness that were not assessed by *a priori* ROIs. ROI-based and voxelwise analyses both present distinct advantages and weaknesses. Voxelwise analysis is not constrained by the borders of anatomically-defined ROIs, and it allows more precise anatomical localization of effects. However, ROI volume is regarded as a more reliable measure of GM atrophy than cortical thickness (Schwarz *et al.*, 2016). Moreover, voxelwise parametric tests depend on patients' displaying neurodegeneration at the same precise point within a brain area. Thus, ROI-based volumetric analysis may be more sensitive to atrophy if the precise focus of atrophy within a region differs across individuals. Voxelwise analysis did not include hippocampus, where cortical thickness is not well estimated (Han *et al.*, 2006; Gronenschild *et al.*, 2012; Schwarz *et al.*, 2016), but did include entorhinal cortex and parahippocampal gyri. As in ROI-based analysis, we used multiple regression to assess group differences at initial MRI and an LME model to investigate longitudinal atrophy. These voxelwise models used the same regression formulae as ROI-based models, and the LME was implemented in the 3dLME (Chen *et al.*, 2013) function from the Analysis of Functional NeuroImaging (AFNI) software suite. Multiple comparisons correction was performed by first thresholding voxelwise results at p<0.001 (uncorrected), then applying a cluster extent threshold corresponding to a cluster-wise alpha value of 0.05. To calculate cluster extent thresholds, we first estimated spatial auto-correlation from the model residuals using AFNI's 3dFWHMx. We then used the 3dClustSim function, which is based on a Monte Carlo approach (Forman *et al.*, 1995; Cox *et al.*, 2017), to determine the cluster size corresponding to a false-positive rate of 0.05 at a voxelwise threshold of p<0.001 (uncorrected). These simulations indicated a cluster threshold of 73 voxels (i.e., 584 µl) for the baseline MRI model and a threshold of 75 voxels (600 µl) for the longitudinal LME model. For both the baseline effect of group and the group x time interaction, we performed post-hoc contrasts between all groups, which were corrected to cluster-wise p<0.05 using the same method. In the Supplementary Material, we additionally display voxelwise contrasts vs. controls at a lenient threshold of p<0.01, uncorrected for multiple comparisons (Supplementary Figure 3).

Structural connectivity

To investigate associations between atrophy progression and brain connectivity, we related longitudinal atrophy to structural population-average structural connectivity measures computed by Yeh et al. (2018). The decision to use population-average connectivity measures rather than estimating connectivity from patients was based on both practical and conceptual considerations. First, constraining participant selection by the availability of white-matter imaging data would have further reduced sample sizes. Second, white-matter degeneration in patients' brains might adversely affect fiber tractography, leading to false negatives in estimating region-to-region brain connectivity.

Yeh and colleagues reported a whole-brain connectivity matrix (available at http://brain.labsolver.org/) based on diffusion MRI data from 842 healthy participants in the Human Connectome Project; connectivity values represent average anisotropy values for white-matter fiber tracts connecting 65 regions in a modified version of the Automated Anatomical Labeling (AAL) brain parcellation (Tzourio-Mazoyer *et al.*, 2002). Because label boundaries for major cortical structures vary between the AAL and Mindboggle parcellations, we warped the modified AAL atlas into the native acquisition space for each of the T1-weighted scans in the current study and re-computed GM volumes based on this parcellation. An example of the anisotropy-based structural connectivity values reported by Yeh et al. (2018) is shown in Supplementary Table 6 for the areas of greatest overlap with Mindboggle ROIs in the hypothesis-driven analysis described above.

Using the igraph package for R (https://igraph.org/r/), we created an unweighted, undirected graph of structural connectivity from Yeh et al.'s (2018) connectivity matrix, omitting the cerebellum and brainstem to yield a total of 62 nodes (i.e., brain areas). The degree of each node was computed as the number of non-zero white-matter connections with other regions. Self-connections were excluded; thus, the maximum possible degree of a node was 61. As with Mindboggle labels, volumes were normalized by each participants' intracranial volume and converted to a z-score relative to the region-wise mean and standard deviation of the control sample. We calculated annualized change in GM volume over time for each region by subtracting

these z-score volume measures from the first and last available scans for each participant and dividing by the time interval. We then computed a linear mixed effects model with annualized change as the outcome and fixed effects of group, node degree, and the group x degree interaction, covarying for the baseline volume of each region, patients' age at initial MRI, and sex. The average volume of each region (i.e., raw volume divided by intracranial volume) among control participants was also included as a covariate to ensure that variation in node degree did not simply reflect differences in region size. A random intercept was estimated for each participant, and a significance threshold of p<0.05 was used.

Data and availability

Computer code for the current manuscript (including all text, analysis, and visualization of results) is available in the form of Rmarkdown and LaTeX scripts in a public GitHub repository (https://github.com/jeffrey-phillips/naAD-longitudinal.git). Rmarkdown code requires R version 3.4.4 or higher. Investigators who wish to access imaging and clinical data may submit a direct request to the corresponding author.

Results

Table 2: Differences in grey matter volume at initial MRI and longitudinal atrophy in hypothesis-driven analysis of regional brain volumes, relative to matched controls. Hypotheses included selective atrophy of neocortical areas associated with early disease in naAD[10] and of the MTL (hippocampus, entorhinal cortex, and parahippocampal gyrus) in aAD patients. The left and right precentral gyri are included to demonstrate the regional specificity of atrophy. F-statistics indicate the main effect of group at initial MRI scan and the group x time interaction across all scans. Additional columns report z-statistics for pairwise contrasts of each patient group vs. controls. Blue cells indicate significant differences in volume only at initial MRI; red cells indicate significant differences in longitudinal atrophy rates; and green cells indicate differences in both initial volume and longitudinal atrophy, based on a threshold of p<0.05, corrected using the false discovery rate method. n.s.=non-significant; *p<0.05; **p<0.01; ***p<0.001.

A priori association	Region	$F_{First\ MRI}(4,103)$	aAD	lvPPA	PCA	fvAD	$F_{Group\ x\ Time}(4,150)$	aAD	lvPPA	PCA	fvAD
aAD	L entorhinal	7.2***	-3.4	-1.5	-1.5	-0.1	6.7***	-2.2	-3.7	-3.3	-3.9
	R entorhinal	5.5***	-2.6	0.7	-1.9	-0.1	7.4***	-4.1	-2.9	-4.1	-3.0
	L hippocampus	8.4***	-4.6	-3.2	-2.1	-1.6	5.4***	-4.1	-2.9	-2.9	-0.3
	R hippocampus	7.4***	-4.3	-1.7	-3.1	-1.8	4.7***	-3.5	-2.3	-3.4	-1.2
	L parahippocampal	2.8**	-1.7	-2.1	0.1	0.8	5.6***	-3.5	-4.0	-2.6	-2.1
	R parahippocampal	1.6*	-2.2	-0.5	-1.3	-0.3	5.9***	-3.7	-2.5	-4.0	-0.5
lvPPA	L middle temporal	30.5***	-3.0	-7.3	-3.2	-3.0	34.7***	-9.6	-9.2	-6.4	-5.3
	L superior temporal	21.5***	-2.6	-6.8	-2.3	-1.8	17.3***	-4.4	-8.1	-3.7	-2.8
PCA	R angular	14.7***	-2.8	-1.3	-3.9	-3.0	2.4	-1.4	-2.6	-2.5	-1.0
	R precuneus	9.8***	-0.7	-0.5	-4.4	-1.3	13.7***	-6.5	-4.8	-4.5	-0.9
	R superior parietal lobule	16.7***	0.6	0.0	-5.5	-1.7	4.2**	-3.6	-2.7	-2.1	-0.1
	R supramarginal	6.4***	0.2	0.4	-2.6	-0.6	11.2***	-6.5	-3.1	-2.6	-0.5
fvAD	L anterior insula	10.3***	-2.1	-2.6	0.6	-3.4	3.5*	-2.0	-1.6	-0.4	-3.3
	L middle frontal	15.3***	-2.6	-3.8	-2.4	-4.4	8.2***	-3.9	-4.9	-3.8	-2.1
PCA, fvAD	R middle temporal	23.6***	-2.8	-2.7	-5.6	-4.2	44.8***	-11.3	-9.3	-7.5	-6.4
Reference ROI	L precentral	3.4***	0.8	-1.3	-1.4	1.2	3.7***	-3.1	-3.1	-2.1	-1.3
	R precentral	5.4***	0.2	-0.7	-2.9	-0.7	5.0**	-3.3	-3.3	-3.3	-0.6

Hypothesis-driven analysis of ROI volumes

Areas of earlier atrophy in each phenotype

We first assessed both regional volume at initial MRI and longitudinal volume change in each group relative to matched controls in ROIs associated *a priori* with each phenotype. The purpose of this hypothesis-driven analysis was two-fold: first, to dissociate effects of earlier vs. later degeneration that are confounded in cross-sectional studies; and second, to test hypotheses regarding differential rates of atrophy between phenotypes. This analysis identified multiple regions displaying initial atrophy in each phenotype (Table 2), which reflect
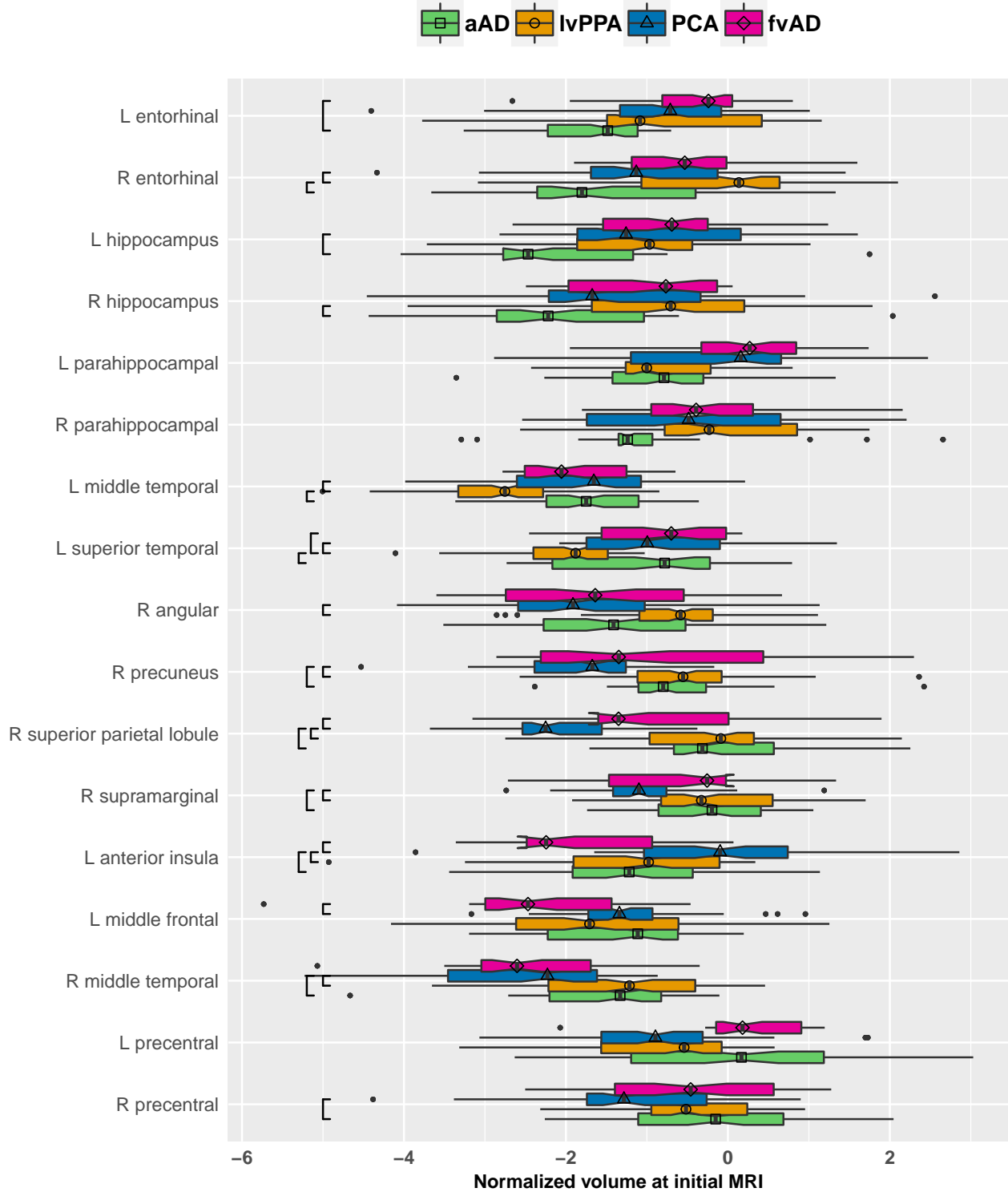
Figure 1: Patient group differences at time of initial MRI in normalized volumes for a priori regions of interest. Box-and-whisker plots represent the distribution of regional grey matter volumes, expressed in z-score units relative to the healthy control reference group and adjusted for age, sex, and global cognition. More negative values on the x-axis indicate greater atrophy. The vertical bar in each box indicates the median volume; the edges of the box represent the interquartile range (IQR), i.e., the difference between the first and third quartiles. The whiskers extend to the most extreme point within $1.5 \times IQR$ from the left or right edge of the box; observations falling outside this range are plotted individually. The notches in each box extend $1.58 \times IQR \div \sqrt{n}$, displaying an approximate 95% confidence interval for the median. Black brackets indicate significant pairwise group differences (p<0.05 after false discovery rate correction). Group is indicated by color as well as by the shape centered over the median line in each box.

atrophy prior to patients' initial scans. While a subset of these regions continued to degenerate over the follow-up period (Table 2, green cells), others exhibited no further change (blue cells). Additionally, we detected a number of regions that were not atrophied relative to controls at the initial scan but demonstrated progression over the follow-up period (red cells); these areas are interpreted as areas of later disease spread in each phenotype. In cross-sectional analysis of participants' initial MRI scans, all ROIs exhibited a main effect of group, independent of age and MMSE.

Patterns of atrophy at initial MRI corroborated prior cross-sectional studies of naAD, supporting the accuracy of clinical diagnoses. LvPPA patients exhibited strong lateralization of disease, with early atrophy relative to controls and other patient groups in left superior and middle temporal gyri (Table 2, Figure 1). Additionally, they had significant atrophy relative to controls in left anterior insula, hippocampus, and middle frontal gyrus as well right middle temporal gyrus. PCA patients, in turn, had significant atrophy at first MRI in right angular gyrus, precuneus, superior parietal lobule, and hippocampus as well as bilateral middle temporal gyri. FvAD patients had significant atrophy in left anterior insula and middle frontal gyrus; right angular gyrus; and bilateral middle temporal gyri. The precentral gyrus, which comprises primary motor areas, exhibited early atrophy only in the PCA group and was restricted to the right hemisphere, consistent with the general right-lateralization of these patients' atrophy pattern; the relative sparing of these structures is consistent with patients' preserved motor function and demonstrates the regional specificity of atrophy patterns. The aAD patients exhibited initial atrophy relative to controls in bilateral hippocampi and entorhinal cortex, left middle frontal gyrus, bilateral temporal cortex, and right angular gyrus. These temporoparietal areas have been previously characterized as nodes of the posterior default mode network in which different AD phenotypes demonstrate convergence of atrophy patterns (Ossenkoppele *et al.*, 2015a). Additionally, aAD patients demonstrated more severe atrophy than naAD groups in bilateral hippocampi and entorhinal cortex (Figure 1). Non-amnestic patients exhibited characteristic sparing of MTL structures, with initial atrophy limited to left hippocampus in lvPPA and right hippocampus in PCA. In longitudinal models, areas of significant early atrophy tended to demonstrate further progression over the follow-up period relative to controls (Table 2, green cells; see also Supplementary Figure 2). However, a subset of brain areas had a non-significant slope of change over time (Table 2, blue cells), suggesting a slowing of atrophy. These areas included left entorhinal and right angular gyrus in aAD; left anterior insula in lvPPA; right superior parietal lobule in PCA; and left middle frontal gyrus in fvAD. Importantly, variation in sample sizes should be taken into consideration when interpreting results for different patient groups. For example, the fvAD group (the smallest sample) may be more susceptible to false negatives than larger groups. We caution against drawing conclusions about group differences by visual comparisons of each group's results vs. controls (Table 2, Figure 3). Rather, group differences in atrophy are directly assessed in Figures 1–2 and 4–5.

Longitudinal analysis identifies areas of later change in each phenotype

Additionally, multiple brain areas in each phenotype demonstrated significant change over time despite an absence of atrophy at initial MRI; these areas appear to represent disease spread in later stages. In the neocortex, lvPPA patients exhibited longitudinal atrophy in right temporoparietal areas, while PCA patients exhibited new left-hemisphere atrophy in superior temporal and middle frontal gyrus. FvAD patients exhibited new atrophy in left superior temporal gyrus, marking lateral temporal cortex as one of the most consistent areas of longitudinal change across patient groups. In the MTL, aAD, lvPPA, and PCA patients all exhibited later atrophy in bilateral parahippocampal gyri; and all three naAD groups demonstrated later atrophy in bilateral entorhinal cortex. Additionally, PCA patients exhibited later-stage atrophy in right hippocampus. Because a subset of PCA patients have a disease focus in the ventral visual processing stream (Crutch *et al.*, 2017), we additionally evaluated longitudinal atrophy in bilateral inferior occipital gyri (Supplementary Tables 7–10); while we observed significant atrophy across patient groups, there were no between-group differences in either mean atrophy or its rate of change. Finally, in precentral gyrus reference regions, all patient groups except fvAD exhibited longitudinal change relative to controls, consistent with their more advanced disease status; however, in the PCA group this change remained restricted to the right hemisphere.

Group differences in regional rates of change

The longitudinal design allowed us to test the hypothesis that each naAD phenotype would exhibit faster atrophy in its associated neocortical ROIs than other patient groups, consistent with phenotype-specific disease patterns. Additionally, we predicted that naAD patients would exhibit more gradual rates of change in MTL structures than aAD patients, providing a dynamic correlate of MTL sparing in naAD. These hypotheses were tested through pairwise contrasts of group x time interaction terms from linear mixed effects models of GM volume change. Consistent with hypotheses, lvPPA patients had more rapid atrophy than PCA patients in left superior temporal gyrus (z=2.8, p<0.02) as well as marginally more rapid change than aAD patients (z=2.1, p<0.09). Similarly, the fvAD group exhibited significantly greater atrophy rates in left anterior insula than lvPPA (z=2.5, p<0.04) and PCA patients (z=2.9, p<0.02). Contrary to hypotheses, PCA patients did not exhibit faster neurodegeneration during the follow-up period than other phenotypes. Because PCA is associated with heterogeneous disease distributions including both dorsal and ventral occipito-temporal variants (Crutch *et al.*, 2017), we performed supplementary analyses of longitudinal atrophy in ventrolateral occipital cortex (i.e., bilateral inferior occipital gyri). While PCA patients exhibited significantly lower GM volumes than controls in both left and right inferior occipital gyri, there were no significant differences in either mean volumes or rates of longitudinal change with other patient groups (Supplementary Tables 7–10).

In addition, aAD patients had more rapid atrophy in right middle temporal gyrus than lvPPA (z=3.5, p<0.01) and PCA patients (z=3.2, p<0.01); in left middle temporal gyrus relative to lvPPA (z=2.7, p<0.03); in right precuneus relative to lvPPA (z=2.5, p<0.04) and fvAD (z=3.0, p<0.02); and in right supramarginal gyrus relative to all three naAD groups (all z>3.3, p<0.01). We had predicted that naAD patients would exhibit more gradual atrophy than aAD patients in MTL structures. However, all patient groups demonstrated significant atrophy relative to controls in one or more MTL structures (Table 2), and we found no significant differences between patient groups in atrophy rates for bilateral hippocampi, entorhinal cortex, or parahippocampal gyri. To address limitations in statistical power, we performed a supplementary analysis on MTL ROIs in which all naAD phenotypes were combined into a single group; while both the naAD and aAD groups had significantly faster atrophy than controls in all 6 MTL regions, we again observed no difference in atrophy rates between naAD and aAD (Supplementary Table 3).

Exploratory whole-brain analysis

Exploratory, whole-brain analysis of cortical thickness was performed to identify areas of early atrophy and later spread that were not captured by *a priori* ROIs. As in ROI analysis (Table 2), areas were categorized by whether they exhibited significant atrophy at patients' first MRI and whether they exhibited significant longitudinal change during the follow-up period relative to controls. As mentioned above, the hippocampi were excluded from voxelwise analysis due to the difficulty of reliably segmenting and estimating cortical thickness for this structure (Han *et al.*, 2006; Gronenschild *et al.*, 2012; Schwarz *et al.*, 2016).

Voxelwise cortical thickness differences at initial MRI

Whole-brain atrophy patterns at initial MRI corroborated ROI-based analyses and indicated areas of earlier neurodegeneration that fell outside of *a priori* ROIs. At initial MRI, the lvPPA group exhibited lower cortical thickness vs. controls in left middle and superior temporal gyri, our hypothesized disease focus for lvPPA, corroborating ROI volume analysis (Figure 3A). In addition to these regions, lvPPA patients exhibited early atrophy in multiple left-hemisphere temporal, parietal, and frontal areas including central and parietal opercula; planum temporale; planum polare; and inferior temporal, fusiform, supramarginal, angular, inferior occipital, and middle occipital gyri (Figure 3). In prefrontal cortex, lvPPA patients had cortical thinning in left anterior insula and frontal operculum as well as bilateral middle and superior frontal gyri. Moreover, nearly all of these areas continued to exhibit longitudinal change during the follow-up period (Figure 3, green areas). Peak t-statistics and cluster volumes for these regions are reported in Supplementary Table 4. Voxelwise analysis of the PCA group not only demonstrated expected atrophy in right parietal, occipital, and posterior temporal areas, but also in their left-hemisphere homologues (Figure 3B). Additionally,
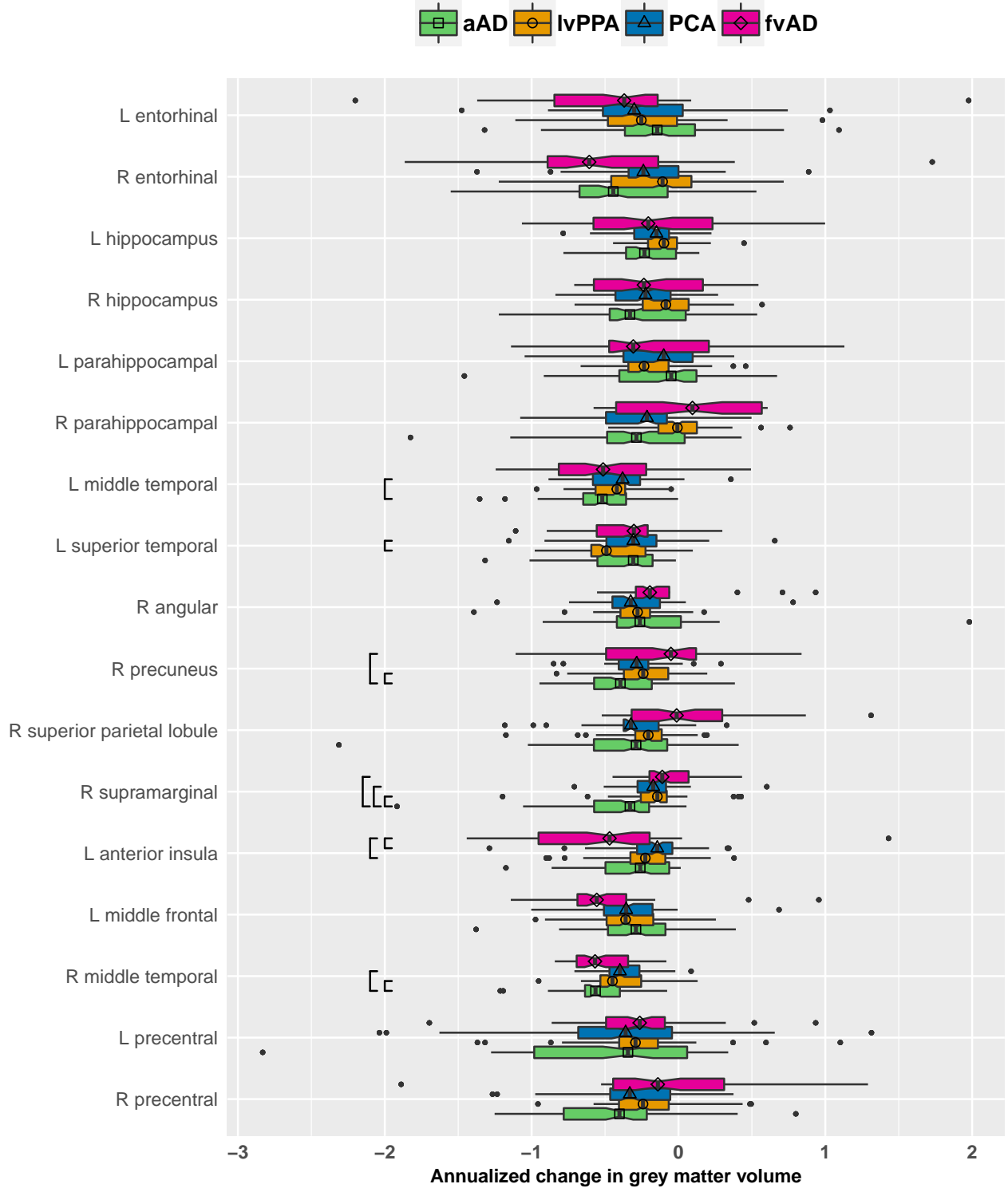
Figure 2: Patient group differences in the effect of time for a priori regions of interest. The plot displays annualized change in regional grey matter volume in each group, expressed in z-score units relative to the healthy control reference group and adjusted for sex as well as age and global cognition at initial MRI. More negative values on the x-axis indicate more rapid atrophy over time. The vertical bar in each box indicates the median volume; the edges of the box represent the interquartile range (IQR), i.e., the difference between the first and third quartiles. The whiskers extend to the most extreme point within $1.5 \times IQR$ from the left or right edge of the box; observations falling outside this range are plotted individually. The notches in each box extend $1.58 \times IQR \div \sqrt{n}$, displaying an approximate 95% confidence interval for the median. Black brackets indicate significant pairwise group differences (p<0.05 after false discovery rate correction). Group is indicated by color as well as by the shape centered over the median line in each box.
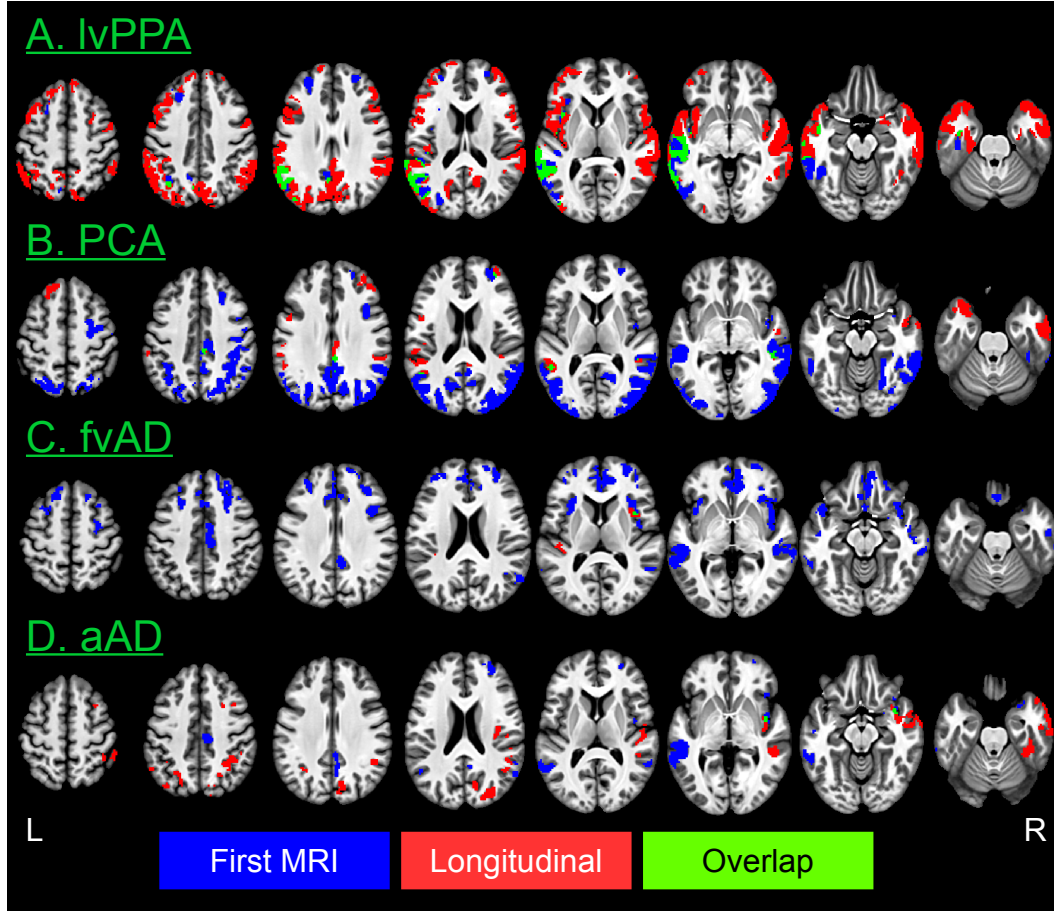
Figure 3: Voxelwise differences in cortical thickness relative to matched controls. Image overlays are binarized t-statistic maps for simple contrasts of controls minus each patient group. Blue: simple effect of group (patients<controls) from cross-sectional analysis of participants' initial MRI scans; red: group x time interaction from longitudinal mixed effects models, indicating where patients have more rapid cortical thinning than controls; green: overlap between group and group x time effects. All results were thresholded at voxelwise p<0.001 with a minimum cluster volume of 584 µl for baseline results and 600 µl longitudinal results, corresponding to a corrected cluster-wise threshold of p<0.05.

PCA patients' baseline atrophy extended into right precentral, middle frontal, and superior frontal gyri. Among these areas, the bilateral precuneus/posterior cingulate gyrus and middle temporal gyrus continued to demonstrate change during the follow-up period. Overall, baseline results thus indicated that despite some right lateralization of disease, PCA patients in the current sample had bilateral cortical involvement consistent with recent consensus criteria for PCA (Crutch *et al.*, 2017). As in ROI-based analysis, fvAD patients exhibited initial atrophy relative to controls in left anterior insula and middle frontal gyrus, right angular gyrus, and bilateral middle temporal gyri. However, areas of early atrophy extended far beyond these regions to include right insula and middle frontal gyrus as well as bilateral medial and ventral prefrontal cortex, inferior and superior frontal gyri, temporal poles, and opercular cortex (Figure 3C). The fvAD group also had initial atrophy relative to controls in the anterior and dorsal portion of right entorhinal cortex, a finding that was not captured by ROI-based analysis. In apparent contrast to the findings of Ossenkoppele and colleagues (Ossenkoppele *et al.*, 2015b), posterior atrophy was limited, most notably including the right precuneus. Among areas of initial atrophy in fvAD, only right anterior insula and bilateral central opercula displayed significant cortical thinning over the follow-up period. The aAD group exhibited expected atrophy in right entorhinal cortex as well as bilateral middle and superior temporal gyri, partially replicating ROI-based findings (Figure 3D). Outside *a priori* ROIs, aAD patients also exhibited early atrophy in bilateral parietal areas including the precunei and middle cingulate, posterior cingulate, angular, and supramarginal gyri; right insula; and right frontal lobe areas including anterior orbital, middle frontal, superior frontal, and medial precentral gyri (Supplementary Table 4). Of these areas, only the right insula demonstrated continued atrophy throughout the follow-up period. Figure 4 presents contrasts between patient groups of initial cortical thickness. Consistent with expectations from previous cross-sectional studies, these results indicate left lateralized atrophy in lvPPA (Figure 4A); parietal and occipitotemporal disease in PCA that exhibits some right-hemisphere bias (Figures 4A, C, and F), and greater frontal lobe involvement in fvAD than in other phenotypes (Figures 4C, E, and F). Collectively, these results replicate initial volume differences from ROI-based analysis and highlight additional phenotype-specific areas of atrophy reported in prior studies of lvPPA (Rogalski *et al.*, 2016), PCA (Lehmann *et al.*, 2012), and fvAD (Whitwell *et al.*, 2011).

Voxelwise whole-brain analysis of longitudinal disease spread

Longitudinal whole-brain analysis also allowed us to identify brain areas that were not significantly atrophied at baseline but demonstrated progressive atrophy over the follow-up period. As in ROI-based analysis, we interpret these effects to indicate the spread of disease to brain areas that were relatively spared in early disease stages. The lvPPA group showed extensive new atrophy in right temporoparietal areas and throughout bilateral prefrontal, medial parietal, and anterior temporal cortex (Figure 3A, red regions), suggesting spread of disease to these areas following patients' initial scans. In PCA, progressive atrophy was observed in several areas unaffected at initial MRI, including the temporal poles, bilateral superior frontal gyri, and bilateral perisylvian cortex (Figure 3B, Supplementary Table 5). In contrast to lvPPA and PCA patients, areas of newer atrophy progression were sparse among fvAD patients, limited to portions of right anterior insula as well as left opercular and perisylvian cortex (Figure 3C). Because the small sample size of this group might have limited statistical sensitivity, we also present voxelwise contrasts vs. controls at a liberal statistical threshold of p<0.01, without cluster-wise correction for multiple comparisons (Supplementary Figure 3). While these results must be interpreted with caution due to the potential for false positive results, they suggest more extensive disease spread to left posterior insula, left dorsolateral prefrontal cortex, and bilateral anterior prefrontal areas. Finally, aAD patients showed new longitudinal change during the follow-up period in bilateral parietal cortex as well as right posterior temporal, anterior temporal, opercular, and prefrontal areas (Figure 3D, Supplementary Table 5).

Voxelwise whole-brain differences in regional rates of change

As in ROI-based analysis, we assessed group differences in the regional pace of cortical thinning over time. Consistent with ROI-based analysis (Figure 2), lvPPA patients had significantly more rapid atrophy than aAD patients in left anterior and posterior superior/middle temporal gyri (Figure 5A). Additionally, aAD patients exhibited faster atrophy progression than fvAD patients in right middle occipital gyrus and superior
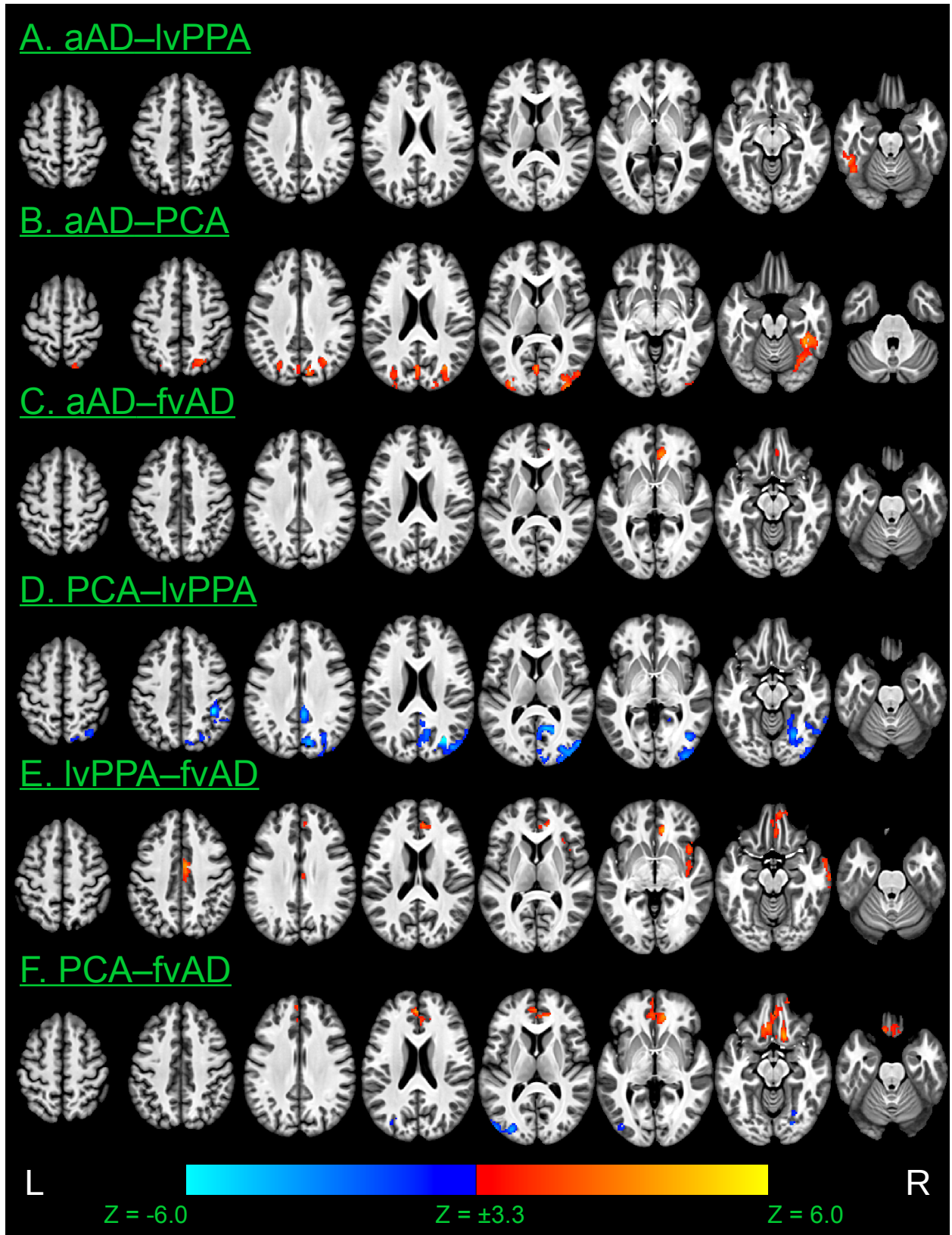
13

Figure 4: Voxelwise differences between patient groups in cortical thickness at time of initial MRI scan. Results are thresholded at voxelwise p<0.001 with a minimum cluster volume of 584 µl, corresponding to a corrected cluster-wise threshold of p<0.05. Warm colors indicate thinner cortical grey matter in the second group than the first; cool colors indicate thinner cortical grey matter in the first group than the second.
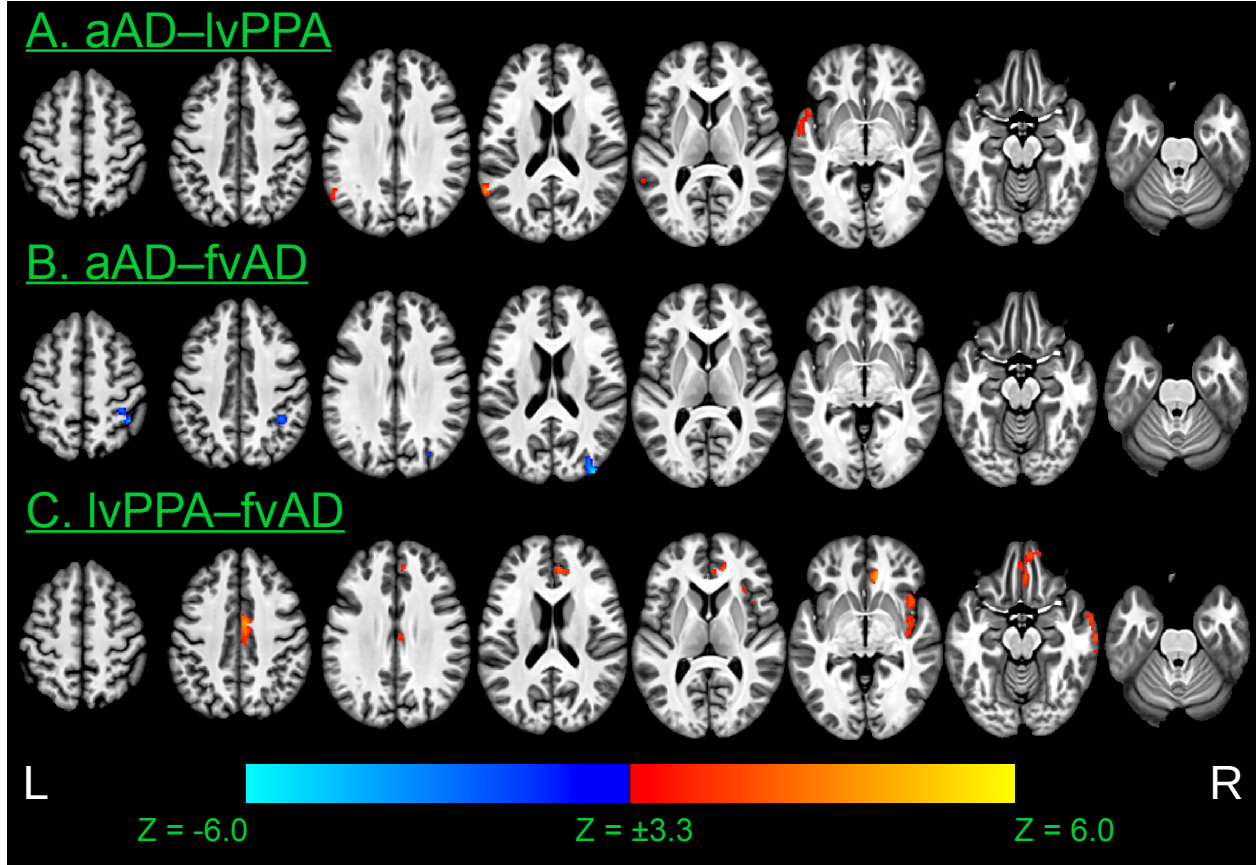
14

Figure 5: Voxelwise differences between patient groups in rates of cortical thinning over time. Image overlays are t-statistic maps for the interaction of each group with time, calculated from linear mixed effects (LME) models and thresholded at voxelwise p<0.001 with a minimum cluster volume of 600 µl, corresponding to a corrected cluster-wise threshold of p<0.05. Warm colors indicate that cortical thinning over time is more rapid in the second group than the first; cool colors indicate that cortical thinning is more rapid in the first group than the second.

parietal lobule (Figure 5B), consistent with parietal differences observed between these groups in ROI-based analysis. Similarly, lvPPA patients exhibited more rapid atrophy than fvAD patients in left precuneus and bilateral middle occipital gyri (Figure 5C). These results corroborate ROI-based findings that suggest neocortical rates of atrophy may vary by region according to patient phenotype.

Degree of structural connectivity predicts longitudinal atrophy

Nodes in the AAL region graph had a median degree of 19.5 (interquartile range=17–25.75). Nodes in the top quartile corresponded to several *a priori* ROIs, including bilateral superior parietal lobules; bilateral inferior, middle, and superior temporal gyri; and right angular gyrus. Both left and right hippocampus labels (which encompassed proximal MTL structures) had degrees of 17; left insula, 23; left middle frontal gyrus, 21; right supramarginal gyrus, 21; right precuneus, 22; and left and right precentral gyri, 21 and 18, respectively. Node degree was positively associated with regions' average volume among controls (Pearson's R=0.46, p<0.001); to account for this potential confound, average control volume for each region was included as a covariate. Linear mixed effects modeling showed that higher node degree predicted greater annualized GM volume loss in each patient group relative to controls (Figure 6), as evidenced by group x degree interaction terms: for lvPPA, β=-0.011, t(6703)=-6.4, p<0.001; for PCA, β=-0.0059, t(6703)=-3.1, p<0.001; for fvAD, β=-0.0049, t(6703)=-2.2, p<0.03; and for aAD, β=-0.010, t(6703)=-5.3, p<0.001. The main effect of degree was marginally significant [β=-0.0020, t(6703)=1.7, p<0.09], reflecting the lack of substantial GM volume loss in the control group (Figure 6). Among covariates, volume at participants' first MRI was significantly associated with annualized change [β=-0.024, t(6703)=-6.2, p<0.001], as was average region size among controls [β=-13.2, t(6703)=-8.3, p<0.001]. Simple effects of group were not significant, although the fvAD group had marginally lower volumes relative to controls [β=-0.15, t(103)=-1.9, p<0.06]. Effects of age and sex were also non-significant (both p>0.12). In pairwise post-hoc contrasts, the aAD group had significantly greater overall volume loss than the lvPPA group (z=2.3, p<0.02). Additionally, the aAD group had a more negative slope of association between degree and longitudinal change than the PCA group (z=2.0, p<0.05) and the fvAD group (z=2.1, p<0.04), suggesting that brain connectivity predicted greater atrophy in aAD than these other phenotypes. Other contrasts of group and group x degree interaction terms were non-significant (all z<0.6, p>0.5). Importantly, these associations were based on GM volumes estimated for AAL labels and are thus unaffected by differences in the AAL and Mindboggle parcellation schemes. Furthermore, because the present analysis relies on population-averaged connectivity values for all groups, it does not address potential connectivity differences between naAD and aAD in networks associated with language, visuospatial function, social behavior, executive control, and memory.

Effects of global cognition and age

Initial MMSE score (which was included as a measure of global cognitive impairment) was positively associated with GM volume in the majority of ROIs [all t(103)>=2.3, p<0.03], with the exception of bilateral hippocampi and parahippocampal gyri [all t(103)<1.0, p>0.3]. In contrast, age at initial MRI was inversely associated with volume in all 6 MTL regions investigated, including left and right hippocampus [t(103)=-2.5, p<0.02 and t(103)=-3.2, p<0.02, respectively, after false discovery rate correction], left and right parahippocampal gyri [t(103)=-3.7, p<0.001 and t(103)=-4.9, p<0.001], and left and right entorhinal cortex [t(103)=-3.2, p<0.002 and t(103)=-3.8, p<0.001]. In addition, age effects were observed in bilateral precentral gyri [both t(103)<-2.9, p<0.01], suggesting age-related atrophy in motor cortex. No other ROIs displayed an effect of age. To determine whether this age effect differed by group, we performed secondary analyses on MTL volumes at the time of first scan using multiple regression models with predictors of group, age, and their interaction, covarying for MMSE score and the interval between MMSE and MRI. After false discovery rate correction, no MTL regions showed a significant group x age interaction [all F(4,99)<2.3, p>0.2], suggesting that the association of increased age with MTL atrophy was similar across groups. Age and MMSE effects for the exploratory voxelwise analysis are shown in Supplementary Figure 1. Consistent with ROI-based results, voxelwise associations with baseline MMSE score were distributed throughout all lobes of the brain (Supplementary Figure 1, bottom). Voxelwise analysis further showed robust age effects in the MTL as well as the precentral gyri, anterior temporal lobes, and ventral prefrontal cortex. Conversely, age was positively
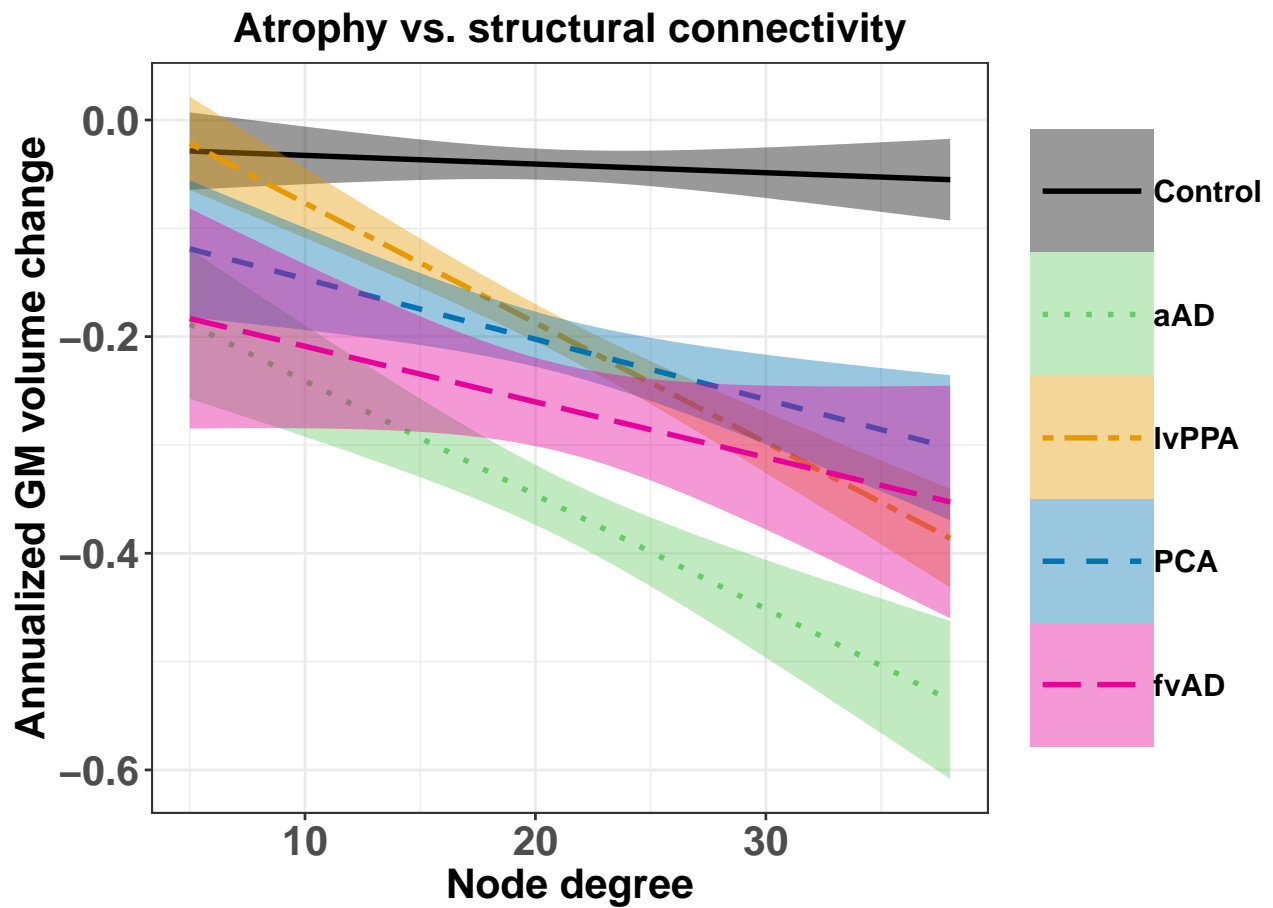
Figure 6: Node degree predicts annualized grey matter volume decline among study participants in regions defined by the Automated Anatomical Labeling (AAL) atlas. Node degree is based on structural connectivity measures computed by Yeh et al. (2018) and reflects the number of white matter connections that each AAL region has with other regions. Shaded areas show the pointwise 95% confidence interval for each regression line.

associated with cortical thickness in the precuneus, which exhibits greater atrophy in earlier-onset than later-onset Alzheimer's disease (Möller *et al.*, 2013). No significant effects of sex were observed in either ROI-based or voxelwise analysis.

Effects of APOE genotype

We additionally assessed the distribution of APOE genotypes among aAD and naAD patients. Genotyping data were unavailable for one lvPPA, one PCA, one fvAD, and two aAD patients. One aAD, three PCA, and three fvAD patients each carried one copy of the $\epsilon 2$ allele, which is associated with lower risk for Alzheimer's disease (Corder *et al.*, 1994). The proportions of lvPPA, PCA, fvAD, and aAD patients carrying 1–2 copies of the APOE $\epsilon 4$ allele were 29.2%, 36.8%, 63.6%, and 73.3%, respectively. The frequency of individuals carrying zero, one, or two copies of the $\epsilon 4$ allele significantly differed across patient groups [$\chi^2(6)$=14.9, p<0.02]. In post-hoc comparisons, these frequencies differed between the lvPPA and PCA groups [$\chi^2(1)$=8.3, p<0.02] and between the PCA and fvAD groups [$\chi^2(1)$=6.1, p<0.05]. Because APOE genotypes were unavailable for control participants, we recomputed LMEs for *a priori* ROIs using lvPPA (the largest group) as the reference group and number of $\epsilon 4$ alleles as a covariate. No ROIs exhibited an association with number of $\epsilon 4$ alleles independent of group (all p>0.2).

Longitudinal associations between neuropsychological performance and grey matter volume

Associations between longitudinal neuropsychological performance and concurrent GM volume loss were evaluated in patients that had two or more assessments, each within one year of a structural MRI scan. This longitudinal analysis contrasts with previous studies that have inferred associations by correlating brain imaging data from a single timepoint with cognitive change. For recognition memory, this yielded 121 observations from 51 patients, including 21 lvPPA, 13 PCA, eight aAD, and nine fvAD patients. For letter fluency, 129 observations were available from 20 lvPPA, 14 PCA, 12 aAD, and nine fvAD patients. For forward and reverse digit span, 117 observations were available from 21 lvPPA, 13 PCA, eight aAD, and eight fvAD patients. A total of 90 PBAC observations, from which all other test measures were obtained, were available for 17 lvPPA, 11 PCA, seven aAD, and seven fvAD patients. In all cognitive domains except for social behavior, longitudinal cognition was directly associated with GM volume change in one or more associated brain areas, independent of volume at the time of initial MRI (Supplementary Table 12). In the memory domain, volume loss in bilateral hippocampi and left entorhinal predicted declines in recognition discrimination. In the language domain, volume loss in left middle and superior temporal gyri was associated with decreases in letter fluency and forward digit span. In the visuospatial domain, Rey figure copy performance over time was associated with volume loss in right angular, middle temporal, and supramarginal gyrus as well as right precuneus. Judgment of line orientations was likewise associated with right precuneus volume change. No significant associations were found for social behavior; however, left middle frontal gyrus, left anterior insula, and right middle temporal gyrus predicted reverse digit span, a measure of working memory and executive function (Kramer *et al.*, 2003).

Discussion

Our previous work (Phillips *et al.*, 2018) used cross-sectional analyses to identify areas of frequent atrophy in several AD phenotypes, which we hypothesized to be likely regions of disease onset. This approach was inspired by pathological staging studies that have inferred disease progression over time in AD (Braak and Braak, 1991), Parkinson's disease (Braak *et al.*, 2003), and amyotrophic lateral sclerosis (Brettschneider *et al.*, 2013) based on postmortem pathology. However, this cross-sectional design did not allow us to directly observe within-patient effects of earlier vs. later disease progression in each phenotype. The current study compared longitudinal disease progression in multiple clinically-defined naAD phenotypes with autopsy or CSF evidence of Alzheimer's disease pathology. We differentiated earlier and later disease stages through a two-part approach. ROI-based analysis allowed us to focus on GM volume change in the most likely sites of

disease onset for each phenotype (Phillips *et al.*, 2018). A second, exploratory analysis of whole-brain cortical thickness values allowed us to examine disease spread outside this cluster of *a priori* ROIs. In each phenotype, we observed a combination of local spread surrounding areas of early atrophy and distal spread to brain areas that were not significantly atrophied at the beginning of the follow-up period. Both patterns of initial atrophy and subsequent progression differed between phenotypes. We further found that longitudinal rates of neurodegeneration differed across patient groups in phenotype-specific neocortical disease foci, a result which could at least partially account for each phenotype's characteristic disease distribution. In contrast, we observed no evidence of phenotype-dependent differences in atrophy rates within the MTL, although MTL atrophy appeared to begin later in naAD than in aAD. Finally, we found that structural connectivity, assessed by node degree, was a significant predictor of GM volume loss over time in both aAD and naAD; this result supports brain connectivity as a general factor mediating atrophy progression in AD.

Atrophy at initial MRI indicates possible sites of early disease

We hypothesized that each naAD phenotype would be characterized by a distinct pattern of early atrophy, observed through cross-sectional contrasts of patients' first MRI scans. We consider significant baseline atrophy an expected and necessary marker for identifying potential sites of disease onset, although early atrophy alone is not sufficient to determine these onset sites. *A priori* ROIs for each phenotype (including left temporal cortex in lvPPA, posterior temporoparietal cortex in PCA, prefrontal cortex in fvAD, and the MTL in aAD) demonstrated significant initial atrophy, consistent with hypotheses. However, the lvPPA and PCA groups also exhibited lateralized hippocampal atrophy vs. controls at initial MRI; although this atrophy was mild relative to the aAD group (Figure 1), we cannot rule out early, lateralized hippocampal disease in these phenotypes. Longitudinal imaging of patients from earlier disease stages, when atrophy will presumably be more focal than in the current sample, is thus necessary to conclusively determine whether focal neocortical disease precedes, follows, or arises concurrently with MTL disease in these phenotypes. Nevertheless, the current study narrows the field of brain areas where disease is likely to originate in each naAD phenotype, providing a valuable prior constraint on future hypothesis testing. Overall, we propose that the current results are more consistent with the prevailing hypothesis that naAD patients have disease originating in the neocortex, as inferred by cross-sectional or single-group longitudinal imaging studies (Rogalski *et al.*, 2011; Lehmann *et al.*, 2012; Rohrer *et al.*, 2013; Ossenkoppele *et al.*, 2015a; Xia *et al.*, 2017; Phillips *et al.*, 2018) as well as autopsy studies of hippocampal-sparing AD (Giannakopoulos *et al.*, 1994; Murray *et al.*, 2011; Ferreira *et al.*, 2017). Phenotypic variability in initial atrophy patterns (Table 2), including sparing of primary motor cortex at the time of initial MRI, supports the regional specificity of atrophy in naAD patients.

Interestingly, some areas of initial atrophy continued to change over time, while others did not. From the data at our disposal, we cannot say with certainty what differentiates these regions. One statistical explanation is simply that variability prevented reliable detection of longitudinal atrophy in some regions and phenotypes. An alternative, biological explanation is that areas that failed to exhibit further change over the follow-up period (blue areas, Table 2 and Figure 3) had already undergone massive atrophy by the time of patients' first MRI, reaching a plateau determined by the limited amount of remaining GM tissue (Sabuncu *et al.*, 2011; Schuff *et al.*, 2012). The right superior parietal lobule in PCA and left middle frontal gyrus in fvAD may exemplify such slowing: in ROI-based analysis, both regions were severely atrophied at initial MRI and did not significantly progress over time in their respective phenotypes. Further research is needed to determine why the pace of atrophy changes in some areas of early degeneration but not others.

Differences between phenotypic groups in the neocortical spread of atrophy

Areas that exhibited longitudinal atrophy in the absence of initial cross-sectional differences provide a window onto disease spread in each phenotype. In ROI-based analysis, the lvPPA group showed strong left lateralization of atrophy at baseline, consistent with prior studies (Rogalski *et al.*, 2016; Phillips *et al.*, 2018). This pattern included left lateral temporal cortex, an area specifically associated with language deficits in lvPPA (Gorno-Tempini *et al.*, 2011). ROI-based analysis also indicated early atrophy in left prefrontal cortex, anterior insula, and hippocampus; and right lateral temporal areas. Voxelwise analysis indicated atrophy in

left precuneus and right prefrontal cortex as well. Over the follow-up period, we observed new progressive atrophy in brain areas both adjacent to and distal from these areas of initial atrophy. Proximal disease spread was observed throughout the left temporal and parietal lobes as well as bilateral frontal lobes. This proximal atrophy may indicate diffusive spread of pathology through the extracellular medium or along short-distance axonal connections between neighboring cells in cortex (Guo and Lee, 2014). However, we also observed progression through parts of bilateral frontal lobes and right temporoparietal cortex distal from foci of initial atrophy (Figure 3); diffusive spread from adjacent disease areas appears insufficient to account for this progression. Two possible explanations may account for new, distal atrophy progression. First, pathology may have arisen independently in these areas; second, pathogenic proteins may have been transmitted to these areas via long-distance white matter projections, according to the transmission hypothesis of neurodegenerative disease (Guo and Lee, 2014). It is particularly interesting to consider these two possibilities with respect to cross-sectional reports of right temporal atrophy in lvPPA, which—if observed—tends to be much milder than left temporal atrophy. In such cases, it is tempting to infer that right temporal atrophy results from the spread of disease from left to right hemispheres via callosal projections. However, this apparent "progression" may result from a subset of patients having bilateral disease. The current study cannot rule out this possibility, as ROI-based analysis indicated right temporal atrophy that pre-dated lvPPA patients' first MRI (Table 2). Earlier recruitment and longitudinal imaging of patients with language disturbances is thus necessary to conclusively demonstrate interhemispheric disease spread in lvPPA.

The PCA group also exhibited a combination of proximal and distal disease spread. Initial atrophy was observed in bilateral precunei and temporoparietal regions (Figure 3) as well as right hippocampus (Table 2). These parietal areas, in particular, are important to visuospatial processing (Astafiev *et al.*, 2003; Greenberg *et al.*, 2010; Gmeindl *et al.*, 2016) and are consistent with early disease patterns observed in prior studies of PCA (Tang-Wai *et al.*, 2004; Lehmann *et al.*, 2012). In voxelwise analysis, PCA patients had newer atrophy extending from areas of early disease into inferior parietal, posterior temporal, and insular/opercular cortex; they also exhibited spread proximal to areas of prefrontal atrophy observed at baseline. In addition, however, the PCA group exhibited atrophy progression in the anterior temporal lobes distal from any cluster of existing atrophy (Figure 3). This finding suggests testable hypotheses regarding the diffusion of disease-causing agents along fiber pathways that terminate in anterior temporal cortex. These pathways include projections from MTL areas as well as more distal connections via the inferior longitudinal fasciculus to striate and prestriate cortex, which may in turn connect with parietal cortex (Nieuwenhuys *et al.*, 2008).

In the fvAD group, ROI-based and voxelwise analysis collectively indicated GM volume loss at initial MRI in bilateral prefrontal, temporal, and anterior insular cortex as well as right middle cingulate and angular gyri. The involvement of the insula is particularly interesting given this group's behavioral dysfunction, as anterior insula is crucially implicated in primates' emotion (Phan *et al.*, 2002) as well as in empathy and social life (Singer, 2006). The anterior insula is also implicated in behavioral-variant frontotemporal dementia (bvFTD) (Seeley, 2010), and Ossenkoppele et al. (2015a) found that insula was one of the few regions of atrophy specific to behavioral-variant AD (bvAD) patients who were initially misdiagnosed as bvFTD. While our findings suggest early involvement of frontal, temporal, and limbic regions, previous studies of behavioral/dysexecutive AD have shown either predominantly frontal (Blennerhassett *et al.*, 2014) or predominantly temporal (Ossenkoppele *et al.*, 2015a) disease. In ROI-based analysis, the fvAD group demonstrated new atrophy progression only in left perisylvian cortex; voxelwise analysis indicated additional disease progression in bilateral insular/opercular cortex. These findings are located proximally to atrophy clusters observed at first MRI and thus may reflect local, diffusive spread of disease. Although more distal atrophy progression was not observed, we emphasize that null results in this group should be interpreted with extreme caution due to the small sample size; while the reported foci may represent the areas of most robust atrophy in the current sample, true disease progression may be missed due to type II statistical error and may be more anatomically widespread than reported here.

In the aAD group, ROI-based analysis showed new neocortical atrophy in bilateral precentral gyri as well as right temporoparietal cortex (Table 2). Voxelwise analysis similarly indicated neocortical atrophy progression throughout the right temporal lobe as well as in bilateral parietal cortex and right prefrontal cortex. The slight lateralization of disease progression (right hemisphere > left) may be incidental to the current sample, and we do not propose that it is characteristic of amnestic AD generally. However, the results are broadly consistent

with spreading neocortical disease in later Braak stages (Braak and Braak, 1991). Clusters of newer atrophy in right temporal cortex may indicate local, diffusive spread from right angular gyrus, which was atrophied at initial MRI in the aAD group. However, other areas of new progression observed in the voxelwise analysis (Figure 3) are distal from sites of early atrophy and may result from either white-matter-mediated disease spread or *de novo* accumulation of pathology. Notably, structural connectivity data from healthy adults indicates that the superior parietal lobule is connected to the hippocampus and angular gyrus (Supplementary Table 6), both of which exhibited baseline atrophy in the aAD group; newer areas of superior parietal atrophy in aAD may thus result from disease transmission along white-matter pathways connecting these areas.

MTL atrophy in amnestic and non-amnestic phenotypes

At initial MRI, aAD patients demonstrated significant atrophy in bilateral entorhinal cortex and hippocampi, as expected from Braak staging (Braak and Braak, 1991). Bilateral parahippocampal gyri were not atrophied, but they demonstrated significant change over the follow-up period; this pattern of results is consistent with progression from approximate Braak stages IV to V (Whitwell *et al.*, 2008) among our aAD sample. Based on well-characterized patterns of disease spread in aAD, these MTL foci may be the source of disease spread to the neocortex. The hippocampus has well-characterized white-matter connections to posterior cortical areas via the posterior cingulate (Nieuwenhuys *et al.*, 2008; Teipel *et al.*, 2010); these pathways thus represent tracts of interest for investigating the spread of pathogenic proteins to the neocortex.

NaAD patients, in turn, demonstrated relative sparing of MTL structures at baseline. In ROI-based analysis, atrophy was limited to left hippocampus in lvPPA and right hippocampus in PCA; these patterns of lateralization were consistent with the general hemispheric bias observed in both phenotypes. Over the follow-up period, naAD patients demonstrated significant atrophy progression in the MTL (Table 2); in the fvAD group, these changes were limited to bilateral entorhinal cortex, although null findings in other MTL structures may reflect the small size of this group. MTL progression in naAD patients suggests that sparing of the hippocampus and surrounding MTL (a set of clinically-defined syndromes) is a graded rather than an absolute phenomenon, and that naAD patients may become increasingly susceptible to hippocampal degeneration at older ages and in more advanced disease. Indeed, age was a strong predictor of MTL atrophy, as evidenced by both ROI-based results (see above, "Effects of global cognition and age") and voxelwise results (Supplementary Figure 1). We note that while naAD patients tend to be younger than typical aAD patients, the current study controlled for this potential confound both by demographic balancing of groups and by covarying for age in statistical models. Thus, baseline differences between aAD and naAD patients in GM volume within the MTL (Figure 1) were not attributable to age differences between these patient groups. Seminal studies of hippocampal sparing in AD (Giannakopoulos *et al.*, 1994; Murray *et al.*, 2011; Whitwell *et al.*, 2012) grouped patients based on postmortem pathology findings; these studies may not have included patients who initially presented with non-amnestic syndromes but developed hippocampal pathology in later disease.

Differences between phenotypic groups in rates of atrophy progression

The design of the current study not only allowed us to investigate differences between phenotypic groups in the topographical distribution of atrophy but also differences in the rate of atrophy within each region. We reasoned that each phenotype might exhibit more rapid degeneration within its associated disease foci, reflecting phenotype-specific susceptibility to disease (Bergeron *et al.*, 2016; Mattsson *et al.*, 2016) in that area. Among neocortical areas associated with naAD phenotypes, we found evidence to support this reasoning. LvPPA patients demonstrated more rapid atrophy in the left temporal cortex than the PCA group (ROI-based analysis, Figure 2) and the aAD group (voxelwise analysis, Figure 5). FvAD patients, in turn, had more rapid atrophy in left anterior insula than both PCA and lvPPA patients in ROI-based analysis (Figure 2); and voxelwise analysis indicated additional prefrontal, temporal, and insular differences between fvAD and lvPPA (Figure 5C). Contrary to our initial hypotheses, we saw no difference in MTL atrophy rates between aAD and naAD patients, even when all three naAD variants were combined to enhance statistical power. Considered together with aAD patients' significant MTL atrophy at initial MRI, this result suggests that

relative MTL sparing in naAD may result from a delayed onset of degeneration in these structures; but that once neurodegeneration has begun, it proceeds at a similar rate as in aAD. However, we caution that these findings warrant replication in longitudinal studies involving larger sample sizes.

Associations between longitudinal atrophy and brain connectivity

To investigate the possible role of brain connectivity in mediating disease spread, we related patients' atrophy patterns to population-average structural connectivity, as estimated from Human Connectome Project white-matter imaging data (Yeh *et al.*, 2018). Several *a priori* ROIs in the current study corresponded to hubs in Yeh et al.'s structural connectivity matrix, as evidenced by their high node degree. These findings replicate established functional connectivity results that have related the neuroanatomy of AD to brain network hubs including bilateral middle temporal, inferior parietal, and superior parietal cortex (Buckner *et al.*, 2009; Crossley *et al.*, 2014). Moreover, we found that node degree was a significant predictor of regional GM volume loss over time in each of the patient groups. We caution that this result is correlative in nature and does not demonstrate long-distance disease spread along white-matter pathways. Indeed, network influences on neurodegeneration need not be limited to physical transport of pathogenic proteins along white-matter tracts; rather, they may reflect effects such as diaschisis (Chételat, 2018), with disease in one area leading to metabolic and functional disruptions in its network neighbors. Computational analysis of atrophy patterns using network models such as those of Raj and colleagues (2012, 2015), Iturria-Medina et al. (2014), and Hu et al. (2016) offers a more rigorous approach for testing hypotheses regarding disease spread in brain networks. Nevertheless, associations between atrophy and node degree provide supporting evidence for the hypothesis that atrophy progression is mediated by structural connectivity. Importantly, the structural connectivity analysis reported here does not address potential hypotheses regarding connectivity differences in naAD and aAD. Indeed, initial research on this question suggests that the connectivity of specific brain networks may differ between typical and atypical presentations of AD (Lehmann *et al.*, 2015; Whitwell *et al.*, 2015). Because the current study relied on population-averaged structural connectivity values, it was limited to showing a general relationship between degree of connectivity and magnitude of longitudinal change; future analysis of patients' specific connectivity patterns remains a high priority.

Convergence of atrophy in advanced disease

The spread of disease along white-matter pathways may help explain the reported convergence of atrophy patterns across AD phenotypes. For example, Ossenkoppele et al. (2015a) proposed that the common temporoparietal atrophy observed among lvPPA, PCA, early-onset AD, and late-onset AD patients could result from convergent disease in nodes of the posterior default mode network. In support of the convergence hypothesis, we note that aAD and naAD variants alike had common early atrophy and subsequent progression in bilateral temporal cortex (Table 2). These results replicate findings from our previous study (Phillips *et al.*, 2018) of substantial overlap in temporoparietal areas among typical and atypical AD patients. Indeed, this study reported that spatial distributions of atrophy become more similar across phenotypes in later disease phases. At the same time, however, we found that simple logistic regression models could effectively discriminate naAD and AD phenotypes from one another based on atrophy patterns, even in advanced disease (Phillips *et al.*, 2018). Moreover, postmortem studies of AD variants show that regional differences in pathology burden persist among AD variants even until the end of life. One proposal for resolving these apparently conflicting results is the proposal of Warren and colleagues (Warren *et al.*, 2012) that different clinical presentations of AD involve a common temporal, parietal, and frontal network, but that genetic variation or other factors cause the nodes of these networks to be differentially engaged across syndromes.

Conclusions and limitations

Strengths of the current study include a novel comparison of longitudinal anatomical changes in multiple clinically-defined naAD phenotypes using both *a priori* ROI-based and whole-brain voxelwise analyses. The

longitudinal study design allowed us to differentiate areas of earlier and later atrophy and to compare these patterns of disease progression across phenotypes. Moreover, we sought to ensure the comparability of the heterogeneous patient groups included here by controlling for demographic and clinical characteristics both during sample selection and in statistical analysis. The relevance of *a priori* ROIs is supported by analyses showing that longitudinal anatomical change is associated with concurrent domain-specific cognitive decline.

However, one major limitation was the inability to evaluate non-linear atrophy progression in Alzheimer's disease: prior evidence suggests that an initial acceleration due to spreading cumulative damage is followed by a deceleration due to the reduction of intact tissue (Sabuncu *et al.*, 2011; Schuff *et al.*, 2012). Such nonlinearities complicate study design and interpretation in ways that may not be fully addressed by equating patient groups for chronological age and estimated disease duration: for example, in the current study, it is possible that areas of early atrophy in each phenotype (i.e., those exhibiting atrophy at initial MRI) have entered the deceleration phase, while for other phenotypes the same regions may have been imaged during the acceleration phase. Investigating longitudinal change in earlier-stage patients may allow us to observe a more complete trajectory of neurodegeneration, and including a minimum of 3–4 imaging timepoints may allow us to discriminate between linear, quadratic, and sigmoid models of neurodegeneration. Another possible limitation in our findings is statistical power, which is likely to have affected voxelwise analysis more severely than ROI-based analysis due to the much stricter multiple-comparisons correction of the former. Power limitations may thus have resulted in underestimation of disease spread in the relatively small fvAD and aAD groups; we thus emphasize the importance of further longitudinal study, particularly of patients for whom postmortem pathological diagnoses are available to rule out the possibility of co-morbid FTLD or other pathologies. Relatedly, the PBAC behavioral scale did not demonstrate expected worsening of behavioral symptoms over time in the fvAD group; while it is possible that this null result stems from successful treatment of behavioral symptoms through psychiatric medications, future research should strive to include more sensitive measures of behavioral dysfunction. An additional limitation is that patients in the current sample were not selected based on availability of white-matter imaging data, preventing us from performing a structured white matter analysis to support interpretations of disease spread along white matter pathways. The current study was also not designed to investigate associations with the APOE genotype or other genetic risk modifiers for Alzheimer's disease. We found that APOE ϵ4 allele counts added little predictive power to our imaging models after accounting for group effects; however, continued study of the APOE genotype and other genetic risk modifiers in naAD remains an important research aim. Finally, future studies should include patients with corticobasal syndrome due to underlying Alzheimer's disease pathology; insufficient longitudinal data prevented us from including this uncommon naAD phenotype in the current study.

Understanding the neuropathological and clinical heterogeneity of Alzheimer's disease is crucial to understanding the mechanisms of its progression. The current study not only corroborated probable areas of early disease for lvPPA, PCA, and fvAD but also showed that each phenotype has a different pattern of atrophy progression across the cortex. Moreover, we report novel evidence that the longitudinal rate of neocortical atrophy varies by region and phenotype in naAD, reflecting phenotype-specific cognitive decline. In contrast, the rate of MTL atrophy in naAD was similar to that found in aAD, suggesting that early sparing of these structures results from a later onset of MTL atrophy in naAD. Finally, we observed associations between longitudinal atrophy and structural brain connectivity, providing indirect support for models of interregional disease spread in association with white-matter fiber pathways in naAD.

Acknowlededgments

Funding

Competing interests

All authors report that they have no competing interests to disclose.

References

Ahmed Z, Cooper J, Murray TK, Garn K, McNaughton E, Clarke H, et al. A novel in vivo model of tau propagation with rapid and progressive neurofibrillary tangle pathology: The pattern of spread is determined by connectivity, not proximity. Acta Neuropathologica 2014; 127: 667–683.

Astafiev SV, Shulman GL, Stanley CM, Snyder AZ, Van Essen DC, Corbetta M. Functional Organization of Human Intraparietal and Frontal Cortex for Attending, Looking, and Pointing. The Journal of Neuroscience 2003; 23: 4689–4699.

Avants BB, Tustison NJ, Song G, Cook PA, Klein A, Gee JC. A reproducible evaluation of ANTs similarity metric performance in brain image registration. NeuroImage 2011; 54: 2033–2044.

Avants BB, Tustison NJ, Stauffer M, Song G, Wu B, Gee JC. The Insight ToolKit image registration framework [Internet]. Frontiers in Neuroinformatics 2014; 8[cited 2015 Jun 26] Available from: http://www.ncbi.nlm.nih.gov/pmc/articles/PMC4009425/

Bergeron D, Bensaïdane R, Laforce R. Untangling Alzheimer's Disease Clinicoanatomical Heterogeneity Through Selective Network Vulnerability - An Effort to Understand a Complex Disease. Current Alzheimer Research 2016; 13: 589–596.

Blennerhassett R, Lillo P, Halliday GM, Hodges JR, Kril JJ. Distribution of pathology in frontal variant Alzheimer's disease. Journal of Alzheimer's disease: JAD 2014; 39: 63–70.

Braak H, Braak E. Neuropathological stageing of Alzheimer-related changes. Acta neuropathologica 1991; 82: 239–259.

Braak H, Del Tredici K, Rüb U, Vos RAI de, Jansen Steur ENH, Braak E. Staging of brain pathology related to sporadic Parkinson's disease. Neurobiology of Aging 2003; 24: 197–211.

Brettschneider J, Del Tredici K, Toledo JB, Robinson JL, Irwin DJ, Grossman M, et al. Stages of pTDP-43 pathology in amyotrophic lateral sclerosis. Annals of neurology 2013; 74: 20–38.

Buckner RL, Sepulcre J, Talukdar T, Krienen FM, Liu H, Hedden T, et al. Cortical Hubs Revealed by Intrinsic Functional Connectivity: Mapping, Assessment of Stability, and Relation to Alzheimer's Disease. Journal of Neuroscience 2009; 29: 1860–1873.

Byun MS, Kim SE, Park J, Yi D, Choe YM, Sohn BK, et al. Heterogeneity of Regional Brain Atrophy Patterns Associated with Distinct Progression Rates in Alzheimer's Disease. PloS One 2015; 10: e0142756.

Chen G, Saad ZS, Britton JC, Pine DS, Cox RW. Linear mixed-effects modeling approach to FMRI group analysis. NeuroImage 2013; 73: 176–190.

Chételat G. Multimodal Neuroimaging in Alzheimer's Disease: Early Diagnosis, Physiopathological Mecha-

nisms, and Impact of Lifestyle. Journal of Alzheimer's Disease 2018; 64: S199–S211.

Corder EH, Saunders AM, Risch NJ, Strittmatter WJ, Schmechel DE, Gaskell PC, et al. Protective effect of apolipoprotein E type 2 allele for late onset Alzheimer disease. Nature Genetics 1994; 7: 180–184.

Cox RW, Chen G, Glen DR, Reynolds RC, Taylor PA. FMRI Clustering in AFNI: False-Positive Rates Redux. Brain Connectivity 2017; 7: 152–171.

Crossley NA, Mechelli A, Scott J, Carletti F, Fox PT, McGuire P, et al. The hubs of the human connectome are generally implicated in the anatomy of brain disorders. Brain 2014; 137: 2382–2395.

Crutch SJ, Lehmann M, Schott JM, Rabinovici GD, Rossor MN, Fox NC. Posterior cortical atrophy. The Lancet Neurology 2012; 11: 170–178.

Crutch SJ, Schott JM, Rabinovici GD, Murray M, Snowden JS, Flier WM van der, et al. Consensus classification of posterior cortical atrophy [Internet]. Alzheimer's & Dementia 2017[cited 2017 Mar 7] Available from: http://www.sciencedirect.com/science/article/pii/S1552526017300407

Dickerson BC, McGinnis SM, Xia C, Price BH, Atri A, Murray ME, et al. Approach to atypical Alzheimer's disease and case studies of the major subtypes. CNS spectrums 2017; 22: 439–449.

Duara R, Loewenstein DA, Shen Q, Barker W, Greig MT, Varon D, et al. Regional patterns of atrophy on MRI in Alzheimer's disease: Neuropsychological features and progression rates in the ADNI cohort. Advances in Alzheimer's Disease 2013; 02: 135–147.

Dubois B, Feldman HH, Jacova C, Hampel H, Molinuevo JL, Blennow K, et al. Advancing research diagnostic criteria for Alzheimer's disease: The IWG-2 criteria. The Lancet Neurology 2014; 13: 614–629.

Ferreira D, Verhagen C, Hernández-Cabrera JA, Cavallin L, Guo C-J, Ekman U, et al. Distinct subtypes of Alzheimer's disease based on patterns of brain atrophy: Longitudinal trajectories and clinical applications. Scientific Reports 2017; 7: 46263.

Forman SD, Cohen JD, Fitzgerald M, Eddy WF, Mintun MA, Noll DC. Improved assessment of significant activation in functional magnetic resonance imaging (fMRI): Use of a cluster-size threshold. Magnetic Resonance in Medicine 1995; 33: 636–647.

Galton CJ, Patterson K, Xuereb JH, Hodges JR. Atypical and typical presentations of Alzheimer's disease: A clinical neuropsychological, neuroimaging and pathological study of 13 cases. Brain: A Journal of Neurology 2000; 123: 484–498.

Giannakopoulos P, Hof PR, Bouras C. Alzheimer's disease with asymmetric atrophy of the cerebral hemispheres: Morphometric analysis of four cases. Acta Neuropathologica 1994; 88: 440–447.

Giannini LAA, Irwin DJ, McMillan CT, Ash S, Rascovsky K, Wolk DA, et al. Clinical marker for Alzheimer disease pathology in logopenic primary progressive aphasia. Neurology 2017; 88: 2276–2284.

Gmeindl L, Chiu Y-C, Esterman MS, Greenberg AS, Courtney SM, Yantis S. Tracking the Will to Attend: Cortical Activity Indexes Self-Generated, Voluntary Shifts of Attention. Attention, perception & psychophysics 2016; 78: 2176–2184.

Gorno-Tempini ML, Hillis AE, Weintraub S, Kertesz A, Mendez M, Cappa SF, et al. Classification of primary progressive aphasia and its variants. Neurology 2011; 76: 1006–1014.

Greenberg AS, Esterman M, Wilson D, Serences JT, Yantis S. Control of Spatial and Feature-Based Attention in Frontoparietal Cortex. The Journal of Neuroscience 2010; 30: 14330–14339.

Gronenschild EHBM, Habets P, Jacobs HIL, Mengelers R, Rozendaal N, Os J van, et al. The Effects of FreeSurfer Version, Workstation Type, and Macintosh Operating System Version on Anatomical Volume and Cortical Thickness Measurements. PLOS ONE 2012; 7: e38234.

Guo JL, Lee VMY. Cell-to-cell transmission of pathogenic proteins in neurodegenerative diseases. Nature

Medicine 2014; 20: 130–138.

Han X, Jovicich J, Salat D, Kouwe A van der, Quinn B, Czanner S, et al. Reliability of MRI-derived measurements of human cerebral cortical thickness: The effects of field strength, scanner upgrade and manufacturer. NeuroImage 2006; 32: 180–194.

Hu C, Hua X, Ying J, Thompson PM, Fakhri GE, Li Q. Localizing Sources of Brain Disease Progression with Network Diffusion Model. IEEE journal of selected topics in signal processing 2016; 10: 1214–1225.

Iba M, Guo JL, McBride JD, Zhang B, Trojanowski JQ, Lee VM-Y. Synthetic Tau Fibrils Mediate Transmission of Neurofibrillary Tangles in a Transgenic Mouse Model of Alzheimer's-like Tauopathy. The Journal of neuroscience : the official journal of the Society for Neuroscience 2013; 33: 1024–1037.

Irwin DJ, McMillan CT, Toledo JB, Arnold SE, Shaw LM, Wang L-S, et al. Comparison of cerebrospinal fluid levels of tau and Aβ 1-42 in Alzheimer disease and frontotemporal degeneration using 2 analytical platforms. Archives of Neurology 2012; 69: 1018–1025.

Iturria-Medina Y, Sotero RC, Toussaint PJ, Evans AC, Alzheimer's Disease Neuroimaging Initiative. Epidemic spreading model to characterize misfolded proteins propagation in aging and associated neurodegenerative disorders. PLoS computational biology 2014; 10: e1003956.

Johnson JK, Head E, Kim R, Starr A, Cotman CW. Clinical and pathological evidence for a frontal variant of Alzheimer disease. Archives of Neurology 1999; 56: 1233–1239.

Klein A, Andersson J, Ardekani BA, Ashburner J, Avants B, Chiang M-C, et al. Evaluation of 14 nonlinear deformation algorithms applied to human brain MRI registration. Neuroimage 2009; 46: 786–802.

Klein A, Ghosh SS, Bao FS, Giard J, Häme Y, Stavsky E, et al. Mindboggling morphometry of human brains. PLOS Computational Biology 2017; 13: e1005350.

Klein A, Tourville J. 101 labeled brain images and a consistent human cortical labeling protocol. Frontiers in Neuroscience 2012; 6: 171.

Kramer JH, Jurik J, Sha SJ, Rankin KP, Rosen HJ, Johnson JK, et al. Distinctive neuropsychological patterns in frontotemporal dementia, semantic dementia, and Alzheimer disease. Cognitive and Behavioral Neurology: Official Journal of the Society for Behavioral and Cognitive Neurology 2003; 16: 211–218.

Lee SE, Rabinovici GD, Mayo MC, Wilson SM, Seeley WW, DeArmond SJ, et al. Clinicopathological correlations in corticobasal degeneration. Annals of neurology 2011; 70: 327–340.

Lehmann M, Barnes J, Ridgway GR, Ryan NS, Warrington EK, Crutch SJ, et al. Global gray matter changes in posterior cortical atrophy: A serial imaging study. Alzheimer's & Dementia 2012; 8: 502–512.

Lehmann M, Madison C, Ghosh PM, Miller ZA, Greicius MD, Kramer JH, et al. Loss of functional connectivity is greater outside the default mode network in nonfamilial early-onset Alzheimer's disease variants. Neurobiology of Aging 2015; 36: 2678–2686.

Libon DJ, Bondi MW, Price CC, Lamar M, Eppig J, Wambach DM, et al. Verbal Serial List Learning in Mild Cognitive Impairment: A Profile Analysis of Interference, Forgetting, and Errors. Journal of the International Neuropsychological Society 2011a; 17: 905–914.

Libon DJ, Rascovsky K, Gross RG, White MT, Xie SX, Dreyfuss M, et al. The Philadelphia Brief Assessment of Cognition (PBAC): A Validated Screening Measure for Dementia. The Clinical Neuropsychologist 2011b; 25: 1314–1330.

Liu L, Drouet V, Wu JW, Witter MP, Small SA, Clelland C, et al. Trans-synaptic spread of tau pathology in vivo. PloS One 2012; 7: e31302.

Marcus DS, Wang TH, Parker J, Csernansky JG, Morris JC, Buckner RL. Open Access Series of Imaging Studies (OASIS): Cross-sectional MRI data in young, middle aged, nondemented, and demented older adults. Journal of Cognitive Neuroscience 2007; 19: 1498–1507.

Mattsson N, Schott JM, Hardy J, Turner MR, Zetterberg H. Selective vulnerability in neurodegeneration:

Insights from clinical variants of Alzheimer's disease. Journal of Neurology, Neurosurgery, and Psychiatry 2016; 87: 1000–1004.

McKhann GM, Knopman DS, Chertkow H, Hyman BT, Jack Jr. CR, Kawas CH, et al. The diagnosis of dementia due to Alzheimer's disease: Recommendations from the National Institute on Aging-Alzheimer's Association workgroups on diagnostic guidelines for Alzheimer's disease. Alzheimer's & Dementia 2011; 7: 263–269.

McMillan CT, Irwin DJ, Nasrallah I, Phillips JS, Spindler M, Rascovsky K, et al. Multimodal evaluation demonstrates in vivo 18F-AV-1451 uptake in autopsy-confirmed corticobasal degeneration. Acta neuropathologica 2016; 132: 935–937.

Medaglia JD, Huang W, Segarra S, Olm C, Gee J, Grossman M, et al. Brain network efficiency is influenced by the pathologic source of corticobasal syndrome. Neurology 2017; 89: 1373–1381.

Mesulam M-M, Rogalski EJ, Wieneke C, Hurley RS, Geula C, Bigio EH, et al. Primary progressive aphasia and the evolving neurology of the language network. Nature Reviews. Neurology 2014a; 10: 554–569.

Mesulam M-M, Weintraub S, Rogalski EJ, Wieneke C, Geula C, Bigio EH. Asymmetry and heterogeneity of Alzheimer's and frontotemporal pathology in primary progressive aphasia. Brain: A Journal of Neurology 2014b; 137: 1176–1192.

Mezias C, LoCastro E, Xia C, Raj A. Connectivity, not region-intrinsic properties, predicts regional vulnerability to progressive tau pathology in mouse models of disease [Internet]. Acta Neuropathologica Communications 2017; 5[cited 2017 Nov 14] Available from: https://www.ncbi.nlm.nih.gov/pmc/articles/PMC5556602/

Möller C, Vrenken H, Jiskoot L, Versteeg A, Barkhof F, Scheltens P, et al. Different patterns of gray matter atrophy in early- and late-onset Alzheimer's disease. Neurobiology of Aging 2013; 34: 2014–2022.

Murray ME, Graff-Radford NR, Ross OA, Petersen RC, Duara R, Dickson DW. Neuropathologically defined subtypes of Alzheimer's disease with distinct clinical characteristics: A retrospective study. The Lancet. Neurology 2011; 10: 785–796.

Nieuwenhuys R, Voogd J, Voogd J, Huijzen C van, Huijzen C van. The Human Central Nervous System. 4th ed. Berlin: Springer; 2008.

Ossenkoppele R, Cohn-Sheehy BI, La Joie R, Vogel JW, Möller C, Lehmann M, et al. Atrophy Patterns in Early Clinical Stages Across Distinct Phenotypes of Alzheimer's Disease. Human brain mapping 2015a; 36: 4421–4437.

Ossenkoppele R, Pijnenburg YAL, Perry DC, Cohn-Sheehy BI, Scheltens NME, Vogel JW, et al. The behavioural/dysexecutive variant of Alzheimer's disease: Clinical, neuroimaging and pathological features. Brain 2015b; 138: 2732–2749.

Peter J, Abdulkadir A, Kaller C, Kümmerer D, Hüll M, Vach W, et al. Subgroups of Alzheimer's disease: Stability of empirical clusters over time. Journal of Alzheimer's disease: JAD 2014; 42: 651–661.

Phan KL, Wager T, Taylor SF, Liberzon I. Functional neuroanatomy of emotion: A meta-analysis of emotion activation studies in PET and fMRI. NeuroImage 2002; 16: 331–348.

Phillips JS, Da Re F, Dratch L, Xie SX, Irwin DJ, McMillan CT, et al. Neocortical origin and progression of gray matter atrophy in nonamnestic Alzheimer's disease. Neurobiology of Aging 2018; 63: 75–87.

Poulakis K, Pereira JB, Mecocci P, Vellas B, Tsolaki M, Link to external site this link will open in a new window, et al. Heterogeneous patterns of brain atrophy in Alzheimer's disease. Neurobiology of Aging 2018; 65: 98–108.

Raj A, Kuceyeski A, Weiner M. A Network Diffusion Model of Disease Progression in Dementia. Neuron 2012; 73: 1204–1215.

Raj A, LoCastro E, Kuceyeski A, Tosun D, Relkin N, Weiner M. Network Diffusion Model of Progression Predicts Longitudinal Patterns of Atrophy and Metabolism in Alzheimer's Disease. Cell Reports 2015; 10:

359–369.

Ramanan S, Bertoux M, Flanagan E, Irish M, Piguet O, Hodges JR, et al. Longitudinal Executive Function and Episodic Memory Profiles in Behavioral-Variant Frontotemporal Dementia and Alzheimer's Disease. Journal of the International Neuropsychological Society: JINS 2017; 23: 34–43.

Rascovsky K, Hodges JR, Knopman D, Mendez MF, Kramer JH, Neuhaus J, et al. Sensitivity of revised diagnostic criteria for the behavioural variant of frontotemporal dementia. Brain 2011; 134: 2456–2477.

Rascovsky K, Salmon DP, Hansen LA, Thal LJ, Galasko D. Disparate letter and semantic category fluency deficits in autopsy-confirmed frontotemporal dementia and Alzheimer's disease. Neuropsychology 2007; 21: 20–30.

Rogalski E, Cobia D, Harrison TM, Wieneke C, Weintraub S, Mesulam M-M. Progression of language decline and cortical atrophy in subtypes of primary progressive aphasia. Neurology 2011; 76: 1804–1810.

Rogalski E, Sridhar J, Rader B, Martersteck A, Chen K, Cobia D, et al. Aphasic variant of Alzheimer disease: Clinical, anatomic, and genetic features. Neurology 2016; 87: 1337–1343.

Rohrer JD, Caso F, Mahoney C, Henry M, Rosen HJ, Rabinovici G, et al. Patterns of longitudinal brain atrophy in the logopenic variant of primary progressive aphasia. Brain and Language 2013; 127: 121–126.

Sabuncu MR, Desikan RS, Sepulcre J, Yeo BTT, Liu H, Schmansky NJ, et al. The Dynamics of Cortical and Hippocampal Atrophy in Alzheimer Disease. Archives of Neurology 2011; 68: 1040–1048.

Schuff N, Tosun D, Insel PS, Chiang GC, Truran D, Aisen PS, et al. Nonlinear time course of brain volume loss in cognitively normal and impaired elders. Neurobiology of Aging 2012; 33: 845–855.

Schwarz CG, Gunter JL, Wiste HJ, Przybelski SA, Weigand SD, Ward CP, et al. A large-scale comparison of cortical thickness and volume methods for measuring Alzheimer's disease severity. NeuroImage: Clinical 2016; 11: 802–812.

Seeley WW. Anterior insula degeneration in frontotemporal dementia. Brain Structure & Function 2010; 214: 465–475.

Shaw LM, Vanderstichele H, Knapik-Czajka M, Clark CM, Aisen PS, Petersen RC, et al. Cerebrospinal fluid biomarker signature in Alzheimer's disease neuroimaging initiative subjects. Annals of Neurology 2009; 65: 403–413.

Singer T. The neuronal basis and ontogeny of empathy and mind reading: Review of literature and implications for future research. Neuroscience and Biobehavioral Reviews 2006; 30: 855–863.

Tang-Wai DF, Graff-Radford NR, Boeve BF, Dickson DW, Parisi JE, Crook R, et al. Clinical, genetic, and neuropathologic characteristics of posterior cortical atrophy. Neurology 2004; 63: 1168–1174.

Teipel SJ, Bokde ALW, Meindl T, Amaro E, Soldner J, Reiser MF, et al. White matter microstructure underlying default mode network connectivity in the human brain. NeuroImage 2010; 49: 2021–2032.

Toledo JB, Brettschneider J, Grossman M, Arnold SE, Hu WT, Xie SX, et al. CSF biomarkers cutoffs: The importance of coincident neuropathological diseases. Acta neuropathologica 2012; 124: 23–35.

Tustison NJ, Avants BB, Cook PA, Zheng Y, Egan A, Yushkevich PA, et al. N4ITK: Improved N3 bias correction. IEEE transactions on medical imaging 2010; 29: 1310–1320.

Tustison NJ, Avants BB. Explicit B-spline regularization in diffeomorphic image registration [Internet]. Frontiers in Neuroinformatics 2013; 7[cited 2018 Oct 5] Available from: https://www.ncbi.nlm.nih.gov/pmc/articles/PMC3870320/

Tustison NJ, Cook PA, Klein A, Song G, Das SR, Duda JT, et al. Large-scale evaluation of ANTs and FreeSurfer cortical thickness measurements. NeuroImage 2014; 99: 166–179.

Tzourio-Mazoyer N, Landeau B, Papathanassiou D, Crivello F, Etard O, Delcroix N, et al. Automated anatomical labeling of activations in SPM using a macroscopic anatomical parcellation of the MNI MRI

single-subject brain. NeuroImage 2002; 15: 273–289.

Wang H, Suh JW, Das SR, Pluta J, Craige C, Yushkevich PA. Multi-Atlas Segmentation with Joint Label Fusion. IEEE transactions on pattern analysis and machine intelligence 2013; 35: 611–623.

Warren JD, Fletcher PD, Golden HL. The paradox of syndromic diversity in Alzheimer disease. Nature Reviews Neurology 2012; 8: 451–464.

Whitwell JL, Dickson DW, Murray ME, Weigand SD, Tosakulwong N, Senjem ML, et al. Neuroimaging correlates of pathologically defined subtypes of Alzheimer's disease: A case-control study. The Lancet Neurology 2012; 11: 868–877.

Whitwell JL, Jack CR, Przybelski SA, Parisi JE, Senjem ML, Boeve BF, et al. Temporoparietal atrophy: A marker of AD pathology independent of clinical diagnosis. Neurobiology of Aging 2011; 32: 1531–1541.

Whitwell JL, Jones DT, Duffy JR, Strand EA, Machulda MM, Przybelski SA, et al. Working memory and language network dysfunction in logopenic aphasia: A task-free fMRI comparison to Alzheimer's dementia. Neurobiology of aging 2015; 36: 1245–1252.

Whitwell JL, Josephs KA, Murray ME, Kantarci K, Przybelski SA, Weigand SD, et al. MRI correlates of neurofibrillary tangle pathology at autopsy. Neurology 2008; 71: 743–749.

Xia C, Makaretz SJ, Caso C, McGinnis S, Gomperts SN, Sepulcre J, et al. Association of In Vivo [18F]AV-1451 Tau PET Imaging Results With Cortical Atrophy and Symptoms in Typical and Atypical Alzheimer Disease [Internet]. JAMA Neurology 2017[cited 2017 Mar 15] Available from: http://jamanetwork.com/journals/jamaneurology/fullarticle/2604134

Yeh F-C, Panesar S, Fernandes D, Meola A, Yoshino M, Fernandez-Miranda JC, et al. Population-averaged atlas of the macroscale human structural connectome and its network topology. NeuroImage 2018; 178: 57–68.